An Introduction to Stratospheric Chemistry
SURVEY ARTICLE

Darryl J. Chartrand*, Jean de Grandpré and John C. McConnell
Department of Earth and Atmospheric Science
York University, 4700 Keele Street
Toronto, Ontario M3J 1P3

ABSTRACT *This paper is an expansion of the lectures presented by the authors at the Canadian Middle Atmosphere Model (CMAM) summer school, 25–29 August 1997. It attempts to fulfill several goals as did the curriculum for the summer school. Firstly, it has a large tutorial component allowing newcomers a rapid introduction to the field, secondly it surveys the field of stratospheric chemistry, and thirdly it attempts to bring the reader to the forefront of some of the problem areas in stratospheric chemistry. As such, it includes much background information such as the magnitude of rate coefficients, photolysis rates and their calculation and time constants. The intended audience is individuals about to commence study or research in the field of atmospheric chemistry or established atmospheric scientists in other areas wishing to expand their knowledge of this topic.*

The basic chemistry of the ozone layer is described with an emphasis on the catalytic cycles and the equilibria between "reservoir" and "active" species. To this end, a compendium of the important aspects of heterogeneous chemistry is also provided. The application of box (0-dimensional) and more elaborate (1-, 2- and 3-dimensional) models to compare and validate with measurements is discussed. Also, factors affecting the present and future trends in ozone concentration, both at mid-latitudes and in the polar region, are presented.

RÉSUMÉ *Cet article est un développement des conférences données par les auteurs du Modèle Canadien de l'Atmosphère Moyenne (MCAM), dans le cadre d'un cours d'été qui s'est déroulé du 25 au 29 août 1997. Il tente de répondre à plusieurs objectifs comme le fait le programme d'études pour le cours d'été. Il comprend, d'abord, une composante pédagogique importante permettant aux nouveaux venus d'assimiler rapidement l'introduction du sujet enseigné ; en second lieu, il explore le domaine de la chimie stratosphérique; et enfin, il tente d'amener le lecteur à l'avant-garde de quelques problèmes actuels en chimie stratosphérique. On y retrouve beaucoup de documentation sur la grandeur des taux des coefficients, sur les taux de photolyse ainsi que leur calcul, et sur les constantes de temps. L'auditoire visé s'adresse à des individus qui sont sur le point de commencer leurs études ou leur recherche*

dans le domaine de la chimie atmosphérique ou encore à des scientifiques chevronnés de l'atmosphère ou d'autres sciences manifestant un intérêt d'améliorer leur connaissance dans ce domaine.

La chimie de base de la couche d'ozone y est décrite et on met l'accent sur les cycles catalytiques et l'état d'équilibre entre le «réservoir» et les éléments «actifs». Enfin, un recueil des aspects importants de la chimie hétérogène fait aussi partie du document. On a discuté de l'application du modèle de la boîte (0 - dimension) et d'un autre plus élaboré (1 - 2 - 3 - dimensions) pour les comparer et les valider avec des mesures. On a présenté aussi les facteurs affectant les tendances actuelles et futures des concentrations d'ozone, à la fois aux latitudes moyennes et dans les régions polaires.

1 Introduction

Radiative processes (solar heating and infrared cooling) in the stratosphere directly involve ozone and other chemical species in the 15- to 55-km altitude region. Ozone in the stratosphere strongly absorbs radiation in the ultraviolet at wavelengths below 300 nm, and, at these heights, dissipates most of the absorbed energy locally as heat. This leads to an increase in temperature and the formation of temperature gradients which, in turn, affect pressure and dynamics in the stratosphere. The change in the dynamics leads to modification of the transport of O_3 (and other important trace species). For these reasons, ozone concentration calculations are of central importance to global climate modelling of the middle atmosphere, a region lying roughly between the tropopause ($\sim$12 km) and the homopause ($\sim$100 km).

The total amount of ozone and its vertical distribution in the stratosphere are a result of a myriad of chemical processes which are a function of solar (and reflected) radiance at these altitudes as well as the amount of active hydrogen, nitrogen, chlorine and bromine (HO_x, NO_x, ClO_x, BrO_x respectively; see Section 4). These chemical species have both biogenic and anthropogenic origins. Volcanic eruptions, biomass burnings, CFCs, methane, aircraft emissions and climate changes (albedo changes, warming etc.) can also significantly affect the chemical nature of the stratosphere. Thus, the chemistry and the dynamics of the stratosphere are closely intertwined and must be considered together for climate studies. However, for the purposes of this report, we will not discuss transport in detail because it would require a comprehensive tutorial and review.

This report will present the current status of stratospheric chemistry and in particular, the comparison of modelled and measured ozone. Firstly, a brief summary of transport within the stratosphere as well as exchange between the troposphere and stratosphere is presented in Section 2. Section 3 deals generally with chemical and photochemical reactions which occur in the stratosphere (and elsewhere) as well as a summary of the nucleation processes of molecules. In Section 3, we also discuss lifetimes associated with both chemical (in-situ production or loss) and transport-related processes. Section 4 deals with the gas-phase chemistry that is important in this area of the atmosphere, specifically presenting catalytic cycles which alter the balance between "active" ozone-destroying species and more stable and chemically-inert "reservoir" species. Reactions which can occur on liquid and

solid surfaces (heterogeneous chemistry) can also affect this balance and this is presented in Section 5. Section 6 consolidates all this information as we will discuss and compare modelling studies and observations of stratospheric ozone levels at the poles and at mid-latitudes. Finally, a short summary is given in Section 7.

2 Transport

The transport of various species in the stratosphere is governed by the continuity equation

$$\frac{\partial n_i}{\partial t} + \boldsymbol{\nabla} \cdot \boldsymbol{\Phi}_i = P_i - L_i n_i \tag{1}$$

where n_i is the number density, L_i is the loss frequency (s^{-1}), $\boldsymbol{\Phi}_i$ is the flux of the ith species, and P_i is the production rate in molecules cm^{-3} s^{-1}. The terms on the right hand side can include various natural processes such as emissions from volcanic eruptions as well as anthropogenic perturbations such as aircraft emissions.

Given the discrete approximations adopted in modelling dynamical processes such as grids of points, or truncated series of functions, there are always unresolved elements of the flow. These subgridscale motions are often approximated by postulating fluctuations in dynamical elements such as velocity. For transport it is allowed for by assuming fluctuations in the species mixing ratio. Thus the flux term above, may be written in the following form:

$$\boldsymbol{\nabla} \cdot \boldsymbol{\Phi} \longrightarrow \boldsymbol{\nabla} \cdot (n_i \boldsymbol{v}) + \boldsymbol{\nabla} \cdot (\tilde{K} \boldsymbol{\nabla} \cdot f_i) \tag{2}$$

where $f_i = n_i/m$ represents species mixing ratio, m is the background density, $\boldsymbol{v}$ is the wind vector and $\tilde{K}$ is the eddy diffusion tensor, assuming that the fluctuations are proportional to the gradient of the mixing ratio. This last equation describes species transport in terms of resolved advection terms, $\boldsymbol{\nabla} \cdot (n_i \boldsymbol{v})$, and unresolved terms, $\boldsymbol{\nabla} \cdot (\tilde{K} \boldsymbol{\nabla} \cdot f_i)$. When analyzed carefully this last term can be generalized to include various processes such as large-scale convection and diffusion in the planetary boundary layer, all of which occur on scales smaller than can be resolved by current large-scale stratospheric models. These subgridscale transport terms need to be parametrized since they occur at scales which are not resolved by the model. We note that in the stratosphere subgridscale transport is of secondary importance as evidenced by the size of the second term above. Subgridscale terms for chemistry are generally left out because no one as yet has devised a satisfactory way of dealing with them, or even with appropriately evaluating them. However, recent calculations at varying resolutions suggest that it is possible that the mean fluctuations may not be zero, and loss terms may be present (Edouard et al., 1996; Chipperfield et al., 1997).

One of the important time constants associated with the stratosphere which greatly differentiates it from the troposphere is the vertical mixing time which is given approximately by $H^2/K(z)$. H is the pressure scale height (see below) and $K(z)$ is somewhat akin to the vertical component of the eddy diffusion tensor

mentioned above. However, it is really only used in 1D models and so in some vague sense carries information on resolved transport in those simpler models. In the literature $K(z)$ is the one-dimensional (altitude) vertical eddy diffusion coefficient which is usually derived from observations of long-lived tracers such as N_2O or CH_4 (e.g., see Brasseur and Solomon, 1986). It has units of $(length)^2(time)^{-1}$. H, the atmospheric scale height, is given by RT/g where R is the gas constant for air, T is the background temperature and g is the acceleration due to gravity. At the ground H has a value of ~ 8 km. It represents the altitude over which atmospheric pressure decreases by $1/e$. Thus $H^2/K(z)$ has the units of time and gives a crude estimate of the vertical transport time which averages wave and other motions that lead to vertical transport.

The solution to the continuity equation will determine the temporal evolution of the species distribution given the various forcing mechanisms represented. The form of the differential equation is generally complex and can be solved using a wide range of numerical approaches. However, all methods use various approximations to solve the differential equation which will inevitably introduce error into the solution. The main errors consist of a false dispersion where the flow of the constituents is slightly distorted as well as numerical dissipation where small-scale features are simply attenuated. It is often the nature and the scale of the problem to be studied which will determine the most suitable numerical approach to be used.

The most common approaches use Eulerian finite-difference schemes to calculate the various terms of the continuity equation. A variety of high-order schemes have been developed to ensure that the methods conserve the various moments of the solution including mass and variance (Prather, 1986). The semi-Lagrangian technique is also widely used for modern applications to calculate the advection term. This method is somewhat dissipative but can preserve the shape of the transported field with some efficiency (Rasch and Williamson, 1990). The method consists of determining species concentration at any location by using the wind field to estimate the origin of the air parcel reaching it. This technique does not require the complex calculation of the differential terms as with Eulerian approaches but it is necessary to use high-order interpolation schemes to estimate air parcel trajectories and species trajectories.

For some applications where the physical domain is not area-limited, the spectral method is used as an alternative to evaluate the advection term. In this approach, the species distribution is decomposed in finite series of spherical harmonics and substituted in the differential equations to be solved. Given the nature of this approach, global aspects of the species distribution such as the total mass will be well represented. But spectral techniques can also generate undesirable local effects such as ripples in the background distribution as well as producing (unphysical) negative mixing ratios. Gridpoint methods generally include constraints to prevent this type of effect but also to preserve better the shape of species distributions over limited areas. This aspect is crucial for most applications, which explains the relative popularity of this method compared to spectral schemes.

The strong static stability that exists throughout the stratosphere prevents any strong vertical motion and the characteristic timescale for species mixing is usually several months or more. In the troposphere, surface heating establishes much lower static stability which ensures a relatively rapid vertical mixing of species throughout the domain and the timescale can be as short as a few hours in the case of strong convective events. The differences in mixing processes are important enough to create fundamental discrepancies in the chemical composition of two air masses. It can lead to a new characterization of the tropopause in terms of mixing barriers instead of the classical approach which defines it in terms of thermal gradients.

The study of stratosphere-troposphere exchange (STE) processes deals with the mixing of atmospheric constituents across the tropopause. This is the subject of intense research activity since the transport of anthropogenic gases in the troposphere and the mechanism by which it crosses the tropopause and into the stratosphere is at the heart of several environmental concerns. In particular, the influence of anthropogenic activities on stratospheric ozone is of utmost importance.

One of the critical regions of ozone loss is the lower stratosphere, a region in which ozone concentrations are strongly influenced by the effects of transport. However, the subtleties of transport in this region are not well understood. Current theories propose that air enters the stratosphere at the tropical tropopause at $\sim$17–18 km and rises to $\sim$20–25 km (the so called "tropical pipe"; Plumb, 1996). This rising air has a distinct tropical signature and properties, such as the H_2O "tape recorder" effect (Mote et al., 1996) in which the amount of water flowing into the stratosphere is determined by freezing at the tropopause. As the tropopause temperature changes, the amount of water changes and this "marked" air is transported upwards. However, much evidence suggests that there is a two-way exchange of mid-latitude air with tropical air (Volk et al., 1996). In fact, Schoeberl et al. (1997) suggest that the mixing occurs below 20 km. Thus, we have the potential scenario of pollution from mid-latitude supersonic aircraft reaching the tropics and being carried aloft in the tropical pipe where the pollution can do more serious damage to the ozone layer. The extent, direction and sensitivity of the transport is uncertain and a matter for concern. It is quite likely that after the Mt. Pinatubo eruption, some of the decrease in the ozone field was due to changes in the dynamics of the stratosphere which altered the transport of ozone and other species (e.g., Tie et al., 1994).

The calculation of correct ozone concentrations is of utmost importance due to the potential influence on dynamical and radiative processes in the atmosphere, which in turn can lead to climate change. Chemically, ozone concentrations will depend on several factors including other trace species and (the presence or absence of) sunlight. We will first review the chemical reactions which can adjust the relative concentrations of chemical species which can concomitantly change ozone levels.

3 Rates of Change

In the atmosphere, there are a myriad of physical and chemical changes a molecule can undergo. A molecule can change chemically by one of several mechanisms

which can be classified chiefly as unimolecular, bimolecular, termolecular (three-body) or photochemical reactions. The latter is a process by which molecules can be transformed from some quantum state to another by absorption of a photon of appropriate energy; the details of this process as well as the determination of the rate at which a particular molecule dissociates after absorption of a photon will be discussed later. Finally, a molecule can also join with other molecules of the same or different type to form aggregates held together by intermolecular forces. These collections of particles can further coagulate to form larger particles, further condense material onto them or evaporate. Reactions can occur on these particles should they exist long enough for molecules to become adsorbed on their surface or diffuse into them. The rate at which molecules condense and coagulate will be discussed as well as the rate at which such heterogeneous reactions occur.

a *Chemical Reactions*

1 BIMOLECULAR REACTIONS

The most common type of chemical reaction occurs between two particles:

$$A + B \longrightarrow C + D + \Delta H. \tag{3}$$

where ΔH is the enthalpy which is negative for exothermic reactions (heat is evolved) and positive for endothermic reactions (heat source is required). A reaction can proceed spontaneously if the Gibbs free energy:

$$\Delta G = \Delta H - T\Delta S \tag{4}$$

of the process decreases in moving from reactants to products. Therefore, if the enthalpy change ΔH is positive, the reaction will only proceed spontaneously if (i) there is a source of energy nearby or (ii) there is a compensating increase in entropy or randomness. This entropy term is usually much smaller than the enthalpy term (especially at stratospheric temperatures) and to a first approximation, enthalpy will be the determining factor as to whether the reaction proceeds spontaneously or not ($\Delta G \simeq \Delta H$). Exothermic reactions liberate energy and as a result "chemical heating" can be important in the thermal budget of the stratosphere. The change in enthalpy and free energy associated with chemical reactions is not unique to bimolecular reactions but is characteristic of all reactions in the atmosphere.

A quantitative measure of how fast a reaction moves from reactants to products is given by the *rate constant*. As a zeroth-order approximation to calculating rate constants, one considers molecule A as a sphere of radius r_A. If another molecule B has a radius r_B, a collision will only occur if the distance between the centres of the molecules is equal to (or less than) $r_A + r_B$. The area of the circle formed by the sum of the individual radii will then be $\pi(r_A + r_B)^2$ (often called the *collision cross section* area). Since both molecules A and B are moving, we must consider the relative velocity of A and B, which is related to the *reduced mass*:

$$\mu = \frac{m_A m_B}{m_A + m_B} \tag{5}$$

where m_A and m_B are the individual molecular masses. The probability that molecules A and B will cross paths will be proportional to the volume of the cylinder (of radius equal to the collision cross section) swept out in a unit time. This can be calculated using the mean thermal velocity of a particle of reduced mass μ. Assuming a Maxwell-Boltzmann distribution of molecular velocities, the average velocity is:

$$u = \left(\frac{8kT}{\pi\mu} \right)^{1/2}. \tag{6}$$

The rate of collision between molecules A and B will be a function of the number densities times the collision cross section:

$$\text{rate} = n_A n_B \pi (r_A + r_B)^2 u_{AB} = k_{AB} n_A n_B. \tag{7}$$

This cross section is in the order of 3×10^{-15} cm^2 while u is about 3×10^4 cm s^{-1} which gives a zeroth-order estimate of a generic bimolecular rate constant (k_{AB}) of 10^{-10} cm^{-3} s^{-1}. This would be the rate if all molecules of A and B impinging on each other reacted to form products. This, of course, is not the case in reality. A bimolecular rate constant is determined by effects such as energy barriers (if any) and geometry. For neutral particles, the intermolecular forces between the molecules will influence the rate constant. These forces are attractive for moderate to longer distances and the overall effect is to increase the collision cross sections at these distances. For the reaction of ions with neutral species, polarization of the neutral species electron clouds induced by the ions and subsequent attractive forces must be considered. Similar electrostatic attractions (or repulsions) must be considered for two reacting ions.

In general the rate constant for a bimolecular reaction is the product of a geometric factor A and an energy barrier term:

$$k_{AB} = A \exp \left(\frac{-E_a}{R} \frac{1}{T} \right) \tag{8}$$

The factor A is a measure of geometric constraints that must be satisfied before a reaction can occur, i.e., the molecules must be aligned correctly before the reaction can take place.

This factor can be estimated by plotting the rate of a reaction at a series of temperatures and determining the y-intercept or by using collision theory. The parameter E_a is the activation energy of the reaction while R is the ideal gas constant. Any increase in temperature will increase the number of molecular pairs which will have sufficient energy to overcome the barrier, and as such these reactions are temperature sensitive. Often, bimolecular reactions which have a favourable de-

crease in free energy are said to be *thermodynamically* favoured reactions, but the relative magnitude of the geometric factor will determine whether the reaction is *kinetically* favoured. Many reactions occurring in the atmosphere involving free radicals have no activation energy since these species are already energetically unstable and therefore quite reactive.

As mentioned above, some rate constants can be calculated using transition-state or collision theory to a (sometimes) reasonable accuracy, but most atmospheric models use rate constants which are experimentally determined. The rate of destruction of one of the reactants (or rate of production of a product molecule) is monitored with time in order to determine the rate at which the reaction is proceeding. Often, this is accomplished using spectroscopic techniques such as monitoring the emergence or disappearance of a particular vibrational mode signature.
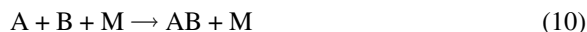
An example of an exothermic reaction is

$$NO_2 + O \rightarrow NO + O_2 \tag{9}$$

The loss term is given by $k[NO_2][O]$ molecules cm^{-3} s^{-1} where $[NO_2]$ and $[O]$ are the number density of the reactants and the units of the second order rate constant k are molecules^{-1} cm^3 s^{-1}.

2 TERMOLECULAR REACTIONS

Termolecular reactions are often written as

$$A + B + M \rightarrow AB + M \tag{10}$$

where M is any third-body molecule (probably N_2 or O_2) and indicates that the reaction is pressure dependent. However, this notation is short hand for the actual process where M is an energy sink for the excited and short-lived AB^* complex. The molecule M is said to *quench* the complex, preventing it from immediately dissociating back to the reactant species.

$$A + B \xrightarrow{k_f} AB^*$$

$$AB^* \xrightarrow{k_r} A + B$$

$$AB^* + M \xrightarrow{k_Q} AB + M \tag{11}$$
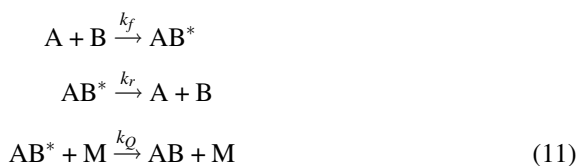
k_r is approximately the vibrational time constant of the complex and is of the order of 10^{12}–10^{13} s^{-1} for simple molecules with few bonds. However, for more complex molecules such as HNO_3, k could be as small as 10^8 s^{-1}. k_f is the bimolecular rate for the formation of AB^*. The "∗" indicates that the molecule has excess vibrational, rotational and possibly electronic energy. We write the rate of formation of AB (molecules cm^{-3} s^{-1})

$$\frac{d[\text{AB}^*]}{dt} = k_{eff}(\text{A})(\text{B}) \tag{12}$$

where

$$k_{eff} = \frac{k_f k_Q(\text{M})}{k_r + k_Q(\text{M})} \,. \tag{13}$$

Note that at low pressures in the upper stratosphere where $\text{M} \rightarrow 0$

$$k_{eff} \cong \frac{k_f k_q}{k_r}(\text{M}) \tag{14}$$

and the rate is explicitly pressure dependent. At higher pressures, for $\text{M} \rightarrow \infty$

$$k_{eff} \cong k_f \tag{15}$$

and the rate constant appears to behave as a two-body rate. Depending on the complexity of the relationship between k_r and k_Q, the three-body reaction can be approximated as a two-body reaction. This transition pressure depends on the reaction.

3 UNIMOLECULAR REACTION

The simplest of all reaction types is represented as

$$\text{A}(+\text{M}) \rightarrow \text{B} + \text{C}(+\text{M}). \tag{16}$$

However, in general and as implied by the (+M) in the above equation, reactions are rarely simply unimolecular. Often, molecule A will form an excited state complex which may or may not be long lived. This "activated" complex (often designated A^*) can then either proceed to form products or can be "deactivated" (or quenched) by transfer of excess energy to another molecule. While the dissociation of the excited complex may be regarded as being unimolecular, the reaction which *forms* the complex may involve two or more molecules and as such the overall rate may be second or higher order.

An important example of a unimolecular decomposition in the stratosphere is:

$$\text{N}_2\text{O}_5 \rightarrow \text{NO}_2 + \text{NO}_3. \tag{17}$$

Tables of the most recent recommended rate constants for many known chemical processes in the stratosphere and many other regions of the atmosphere are given in DeMore et al. (1997).

b *Photochemical reactions*

The photochemistry of the stratosphere is (largely) fuelled by the UV flux of sunlight, I_λ (photons cm^{-2} s^{-1} nm^{-1}), (incident and reflected light from cloud tops)

and consequently the chemistry will depend on the variation of the solar flux with season. For some of the chemistry, the solar insolation (the daily average) is more important. For example, for ozone production, the region of maximum production follows the sun and in the polar regions we have 24 hours of sunlight during the local summer solstice and the result is a maximum in production. Also important is the reduction in intensity of sunlight as it penetrates the atmosphere.

Consider a thin slab of unit area and thickness dz containing molecules of absorption cross section, Q_λ, and number density n. The fractional attenuation of the intensity (dI_λ/I_λ) is given by the projected absorption area of the molecules in the slab, over the (unit) cross sectional area of the slab, viz.

$$\frac{dI_\lambda}{I_\lambda} = -ndzQ_\lambda \tag{18}$$

so that, if Q_λ is independent of pressure and temperature (not always true), the *solar flux* is given by:

$$I_\lambda(z) = I_\lambda^\infty e^{-\tau_\lambda(z)/\cos\chi_\odot} \tag{19}$$

where we have allowed for the slant path through the atmosphere using $\chi_\odot =$ solar zenith angle. Q_λ is an "effective" area that the molecules present to the incoming stream of photons, or the ability of the molecules to attenuate the light. I_λ^∞ is the intensity of unattenuated light of wavelength λ above the atmosphere.

An important quantity is the vertical optical depth

$$\tau_\lambda(z) = \int_z^\infty nQ_\lambda dz \sim Q_\lambda N \tag{20}$$

where $N = \int_z^\infty ndz$ is the vertical column number density above an altitude z. The optical depth represents the projected area of molecules in a column of unit area. Thus when $\tau \sim 1$, the direct solar beam starts to become depleted. The above result describing the variation of the solar intensity with altitude is actually a simplified version. Figures 1a and 1b (DeMore et al., 1997) show the solar flux from 100–600 nm at the edge of the atmosphere and also the solar flux at various depths in the atmosphere. Several important points pertain to the stratosphere: firstly there is a 'window' at about 190–230 nm which allows the penetration of photons with sufficient energy to dissociate O_2 and thus act as the source of ozone production in the stratosphere (see later). The second point is that there is not much attenuation of sunlight beyond 300 nm (visible light region). A last point is that the stratosphere does not receive any sunlight with wavelengths shorter than about 180 nm; these wavelengths are fully attenuated in the mesosphere and the thermosphere.

Air does not interact very strongly with visible electromagnetic radiation and so we can see the sun. For example, if the absorption cross section of air molecules was roughly equal to their collision cross section (see above), $\sim 3 \times 10^{-15}$ cm^2, the optical thickness at the ground, $\tau_\lambda(0) = Q_\lambda N(0)$, would be about $3 \times 10^{-15} \times$
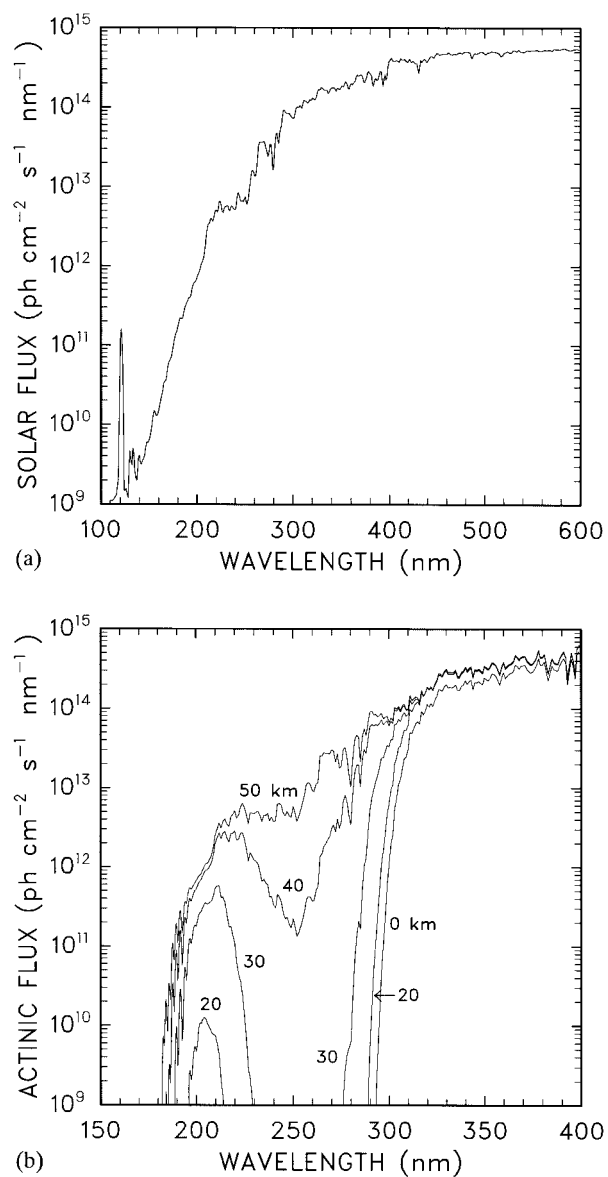
Fig. 1 (a) Plot of solar irradiance as a function of wavelength. Note the large flux at 121.6 nm corresponding to a solar Lyman α line. (b) Actinic solar flux as a function of wavelength and altitude. Below about 200 nm, O_2 in the mesosphere is the primary absorber. Between 200–242 nm, stratospheric O_2 and some O_3 (Hartley band) absorption takes place. Between 242–300 nm, most absorption is due to stratospheric O_3 dissociation leading to $O(^1D)$. From 300–400 nm, the O_3 Huggins bands leading to formation of $O(^3P)$ is the primary absorber. (K. Minschwaner, personal communication).

2.15×10^{25}, or $\sim 6.5 \times 10^{10}$, quite opaque! However, the scattering of light by air molecules is described by Rayleigh scattering but the efficiency of the scattering process, η_R, is exceedingly small, $\sim 10^{-12} - 10^{-13}$. The wavelength dependence of the Rayleigh scattering cross section is described by $Q_{\lambda,R} \sim \frac{1}{\lambda^4}$. The Rayleigh optical depth, i.e., the opaqueness due to air molecules alone, as a function of wavelength and pressure is given by Hansen and Travis (1974):

$$\tau = \frac{8.457 \times 10^{-6}}{\lambda^4} \left[1 + \frac{0.0113}{\lambda^2} + \frac{0.00013}{\lambda^4} \right] p \qquad (21)$$

where λ is in μm and pressure p is in millibars. Thus at the surface for a wavelength of 0.5 μm, say, $\tau \sim 0.14$ and the direct solar beam is only depleted by about 13%.

Scattering of solar radiation by aerosols (particles) is also important in the atmosphere. For the purpose of calculation these droplets, haze particles and sea salt droplets etc. are treated as spherical and Mie scattering theory is applied: it is more anisotropic than Rayleigh scattering with much of the scattered light being directed forward.

Molecules can be destroyed by solar photons and the process can be written similarly to the unimolecular rate for chemical reactions, viz:

$$A + h\nu \longrightarrow B + C + KE \qquad (22)$$

where $h\nu$ represents a photon and KE indicates that the fragments will fly apart with the excess energy, $KE = h\nu - D(A)$, and $D(A)$ is the dissociation energy of the molecule, A. The J value for molecule A is a quantitative measure of this solar interaction. $J[A]$, where $[A]$ is the number density (molecules cm^{-3}) of molecule A, gives the number of photodissociation events per unit volume per unit time. For simplicity, we assume that there is a single species, A, absorbing solar radiation as per the equations above. Thus, for a single wavelength the number of photons absorbed per unit time in the thin slab of volume $1 \times dz$ is given by dI_λ. Each absorption is a photolysis event and the number of events per unit volume per unit time, i.e., $J[A]$ is given by

$$\frac{dI_\lambda}{\text{volume}} = \frac{[A]dzQ_\lambda I_\lambda}{dz} = [A]Q_\lambda I_\lambda = J[A] \qquad (23)$$

The quantity, $Q_\lambda I_\lambda$, is called the J value, or photodissociation rate and has the unit of (time)$^{-1}$. Integrating over the entire spectrum we obtain for the J value

$$J(A, z) = \int_\lambda Q_\lambda I_\lambda d\lambda = \int_\lambda Q_\lambda I_\lambda^\infty e^{-\tau_\lambda / \cos(\chi_\odot)} d\lambda \qquad (24)$$

The J value gives the frequency of occurrence of a photolytic event and its inverse, $1/J$, is a measure of the lifetime of that species against photodissociation.

Figure 2 shows the J value or photolysis coefficients for a number of important species and how they vary with altitude. The values given are for a solar zenith angle
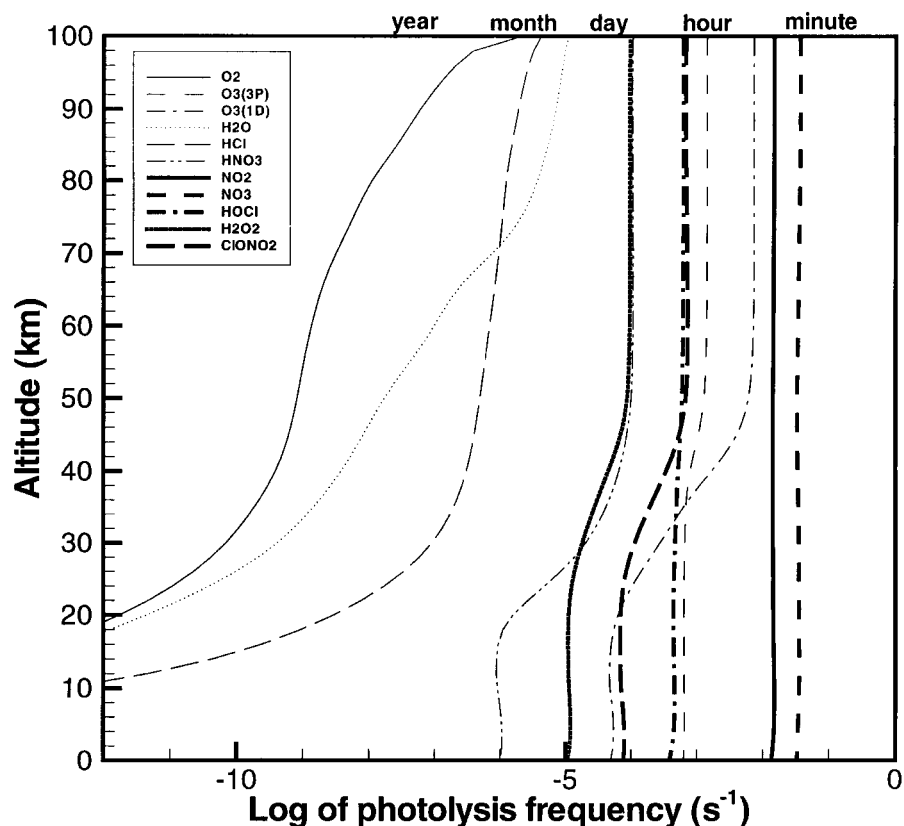
Fig. 2 Photolysis coefficients for a number of important atmospheric species as a function of height. Approximate photolytic lifetimes are shown at the top.

of 0 (impinging photons normal to the tangent of the Earth's surface). In general, there is a decrease in photolysis lifetimes, $1/J$, for the species with increasing height attributable to the fact that there are few absorbers attenuating the higher energy (lower wavelength) photons.

The expressions derived above for the J value only allow for absorption of sunlight: scattering of the photons has been ignored. In fact, we have assumed that the photon field can be described by a plane-parallel beam. However, this is not the case, as scattering from air molecules, aerosols, clouds and the surface will serve to scatter photons. In this case, we must include angular properties in the description of the photon field. We use the radiance, $L_\lambda(\hat{\Omega}; \hat{\Omega}_0; \mathbf{r})$ where L_λ is the number of photons m^{-2} s^{-1} λ^{-1} $ster^{-1}$ crossing normal to surface in the direction $\hat{\Omega}$ at the location $\mathbf{r}$: $\hat{\Omega}_0$ is the Sun angle. The J value is evaluated using the expression for the absorption of photons as above. However, in this case it is given by

$$J(\mathbf{r}, \hat{\mathbf{\Omega}}_\mathbf{o}) = \int_\lambda Q_\lambda J_{av,\lambda}(\mathbf{r}, \hat{\mathbf{\Omega}}_\mathbf{o}) d\lambda \qquad (25)$$

where the solar flux (or irradiance) has been replaced with the angular mean of the radiance, $J_{av,\lambda}$ and

$$J_{av,\lambda}(\mathbf{r}, \hat{\mathbf{\Omega}}_\mathbf{o}) = \frac{1}{4\pi} \int_\Omega L_\lambda(\hat{\mathbf{\Omega}}; \hat{\mathbf{\Omega}}_\mathbf{o}; \mathbf{r}) d\Omega. \qquad (26)$$

Scattering at the surface can be important for enhancing J values depending on the surface. The albedo of the ocean is generally $<10\%$ while that of the surface, or bright clouds can be much larger. For calculations, Lambertian surfaces are often assumed. These are surfaces which reflect the incident light equally in all directions. In the simple case of no atmospheric scattering or absorption but with a Lambertian surface of albedo Λ, the J value is amplified by a factor $(1 + 2\mu_o\Lambda)$ where μ_o is the cosine of the solar zenith angle. Thus for a perfect reflector and an overhead sun, the J value could be amplified by a factor of 3 (McElroy and Hunten, 1966). At the top of a cloudy atmosphere, scattering can increase the photon density so that the J value could be amplified by up to a factor of 5 (e.g., Kaminski and McConnell, 1991). Also it is important to note that the J value enhancement will not just be at the scattering level but at all levels above, if they are optically thin (see also Brasseur and Solomon, 1986).

In general, scattering/reflection is important in the evaluation of J in the stratosphere at wavelengths above $\sim$295 nm, so that it must be known if the air parcel is located above the sea (low albedo, $<10\%$), desert (moderate albedo, $\sim$30%) or cloud (high albedo, $\sim$70–80%). Because of the strong absorption at shorter wavelengths, scattering can generally be ignored. Refraction can also be ignored in the stratosphere under most circumstances.

As noted above, photolysis reactions are first order and we designate the rate constant, which has units of s^{-1}, by J_i. A more general example of such a reaction is:

$$A + h\nu \longrightarrow B + C \qquad E_K + E_R + E_{\text{vibrational}} + E_{\text{electronic}} \qquad (27)$$

where $h\nu$ is representative of a photon of sufficient energy to dissociate the molecule. E_K and E_R represent the kinetic and rotational energy respectively of the products. The exact amount of energy needed to dissociate the molecule will be dependent on the individual molecules and the excited electronic energy quantum states. The more energetic photons can excite the molecule to an another electronic state which may then lead to dissociation. It should be noted here that dissociation may lead to particles which have different electronic states. For instance, the photolysis of molecular oxygen ($\lambda < 175.9$ nm) can lead to production of one O fragment in the ground state ^{3}P and the other in the more energetic and more reactive ^{1}D state. In the middle stratosphere, O(^{1}D) has a very short lifetime of a few nanoseconds while O(^{3}P) has a lifetime of a few hundreths of a second.

The excess energy of the excited atom/molecule may be released locally as heat if quenching by the background gas is rapid. In the upper atmosphere, the number of molecules available to quench the energy of the excited state species decreases.

c *Microphysical Processes*
Particles play a major role in atmospheric physics by acting as nuclei for cloud condensation processes, by acting as scattering and absorbing centres for solar and IR radiation, and by providing surfaces for reactions in the atmosphere. When the particles are small they tend to remain in the atmosphere for a long time either in the stratosphere (few years) or as clouds (hours to days) while large particles (e.g., sea salt aerosols) tend to fall out (sediment) within a few hours. Here we will present some results that pertain to the relation of particles to atmospheric chemistry, particularly stratospheric chemistry.

Sulphuric acid droplets are important in stratospheric chemistry since they act to catalyse the conversion of several species from chemically active to (relatively) inactive forms and vice versa. The process by which sulphuric acid and water join to form a binary solution droplet is thought to be homogeneous nucleation (the direct conversion of gas molecules to condensed phase). The spontaneous formation of a droplet from the vapour phase will occur if the Gibbs free energy (G) of the process decreases (e.g., Seinfeld and Pandis, 1998). The free energy of the formation of a liquid droplet from vapour can be broken down into two terms. First, there is a free energy *decrease* in G as a result of the differences in chemical potential between the vapour and liquid phase molecules ($\mu_v - \mu_l$). Secondly, there is an *increase* in G as a result of the formation of a liquid-vapour interface which is proportional to the surface area of the droplet times the surface tension, $4\pi r^2\sigma$, where r is the droplet radius.

The change in G^* for nucleation of a droplet of radius r^* in (metastable) equilibrium with the vapour can be shown to be (Yue, 1981):

$$\Delta G^* = \frac{4}{3}\pi r^{*2}\sigma \tag{28}$$

where σ is the surface tension per unit area of the new (spherical) droplet. It should be stressed that this new particle is in metastable equilibrium and attachment of another monomer to it will result in further growth by condensation while detachment of a single monomer from the droplet will result in evaporation. This droplet has overcome a free energy barrier and is said to be "activated" while any droplets smaller than this critical-size cluster are classified as "haze" particles.

The droplet can subsequently grow by heteromolecular (water and sulfuric acid) condensation if $P_s - P_s^d > 0$ or evaporate if $P_s - P_s^d < 0$ where P_s in the ambient sulfuric acid vapour pressure and P_s^d is the pressure over the droplet. It is assumed that when sulfuric acid attaches or detaches from the droplet, water will immediately adjust to maintain equilibrium since the number of water vapour molecules (and thus the flux of impinging molecules) is in excess of acid vapour (Yue, 1981).

Assuming that vapour molecules are impinging on a spherical droplet, the rate of change of the particle radius with time is given by (Yue and Hamill, 1979):

$$\frac{dr}{dt} = \frac{\bar{V}_d D(P_s - P_s^d)}{kTrN_s(1 + \lambda K_n)} \tag{29}$$

where $\bar{V}_d$ is the average volume per particle in the droplet, N_s is the number density of sulfuric acid in the droplet. λ is a correction factor (Yue and Hamill, 1979):

$$\lambda \cong \frac{1.333 + 0.71 K_n^{-1}}{1 + K_n^{-1}} \tag{30}$$

where the Knudsen number, $K_n = l_{\text{eff}}/\bar{r}$, and $\bar{r}$ is the average particle radius. The diffusion coefficient (D) of sulfuric acid is (Yue and Hamill, 1979):

$$D = \frac{1}{3} u l_{\text{eff}} \tag{31}$$

where l_{eff} is an effective mean free path. The change in the number of each of the particles making up the droplet is also a function of the gradient between the pressure next to the droplet and the ambient pressure (Fuchs and Sutugin, 1971):

$$\frac{dN_i}{dt} = \frac{4\pi r D(P_s - P_s^d)}{1 + \lambda K_n}. \tag{32}$$

By solving the above equations, the radii of the sulfate aerosols can be calculated assuming the particles grow (shrink) only by homogeneous heteronuclear condensation (evaporation). This assumption is probably not the case since coagulation of larger droplet particles may also lead to growth (Weisenstein et al., 1997). Also, sedimentation of larger aerosol particles may lead to dehydration, the result being less water vapour to participate in the above condensation process, thereby affecting the assumption that water vapour is in constant and rapid equilibrium with condensed phase water.

The rate of gravitational sedimentation is a function of the radius of the particle (r) and is given by Kasten (1968):

$$w = \frac{2}{9} \left(\frac{\rho_p r^2 g}{\eta} \right) \left[1 + \frac{\lambda}{r} \left(A + B \exp \left(\frac{-Cr}{\lambda} \right) \right) \right] \tag{33}$$

where ρ_p is the mass density of the aerosol particle, η is the air viscosity, λ is the mean free path of the falling aerosol and is approximately equal to 0.1 μm at standard pressure and room temperature. A, B and C are empirical constants and are 1.249, 0.42 and 0.87 respectively. Sedimentation rates for aerosol particles of 0.1 μm at 20 km is about 0.0024 cm s^{-1} (2 m day^{-1}); for a typical particle of nitric acid trihydrate (NAT; an important Polar Stratospheric Cloud (PSC) component dealt with in Section 5) of radius 1 μm it is 0.035 cm s^{-1} (30 m day^{-1}), while for

water ice (another PSC particle) of radius 10 μm it is 1.7 cm s^{-1} (1.5 km day^{-1}). Sedimentation of larger PSCs can lead to large decreases in water and nitric acid vapour known as "dehydration" and "denitrification" respectively. It should be noted that for larger particles, the rate of gravitational sedimentation is much larger than the typical rate of vertical transport in the stratosphere (approximately 20 metres per day but is faster in the winter and slower in the summer).

d *Heterogeneous Rate Constants*

If the size of the particles and the number of particles per unit volume of air are known (or assumed), the total volume and surface area in that volume of air can be calculated. The calculation of heterogeneous rate constants is typically done using experimentally determined uptake probabilities (γ). These uptake (or reaction) probabilities are measured for temperatures and gases of atmospheric importance on sulfate aerosols and PSCs. The effective first-order rate constant will then be:

$$k = \frac{\gamma u S}{4} \qquad (34)$$

where u is the mean thermal velocity of the gases impinging on the heterogeneous surface, S is the surface area available on the aerosols and/or PSCs (typically of the order of 0.5–1 cm^2 cm^{-3} for background aerosol conditions and an order of magnitude or more larger for volcanic conditions or when PSCs form). As mentioned, the rates of these types of reactions are assumed to be effectively first order, because the concentration of the species adsorbed on the aerosol surface is held constant in the laboratory at levels similar to that found in the stratosphere. Similarly, determination of reaction probabilities on sulfate aerosols are typically done at temperatures of atmospheric importance (e.g., Donaldson et al., 1997).

In some cases, there is appreciable diffusion of the incident species into the liquid aerosol, and therefore the rate of the reaction will not be strictly dependent on the surface area of the aerosol but on the volume. This will be the case when the reaction is **not** limited by the diffusion of the impinging gas-phase molecules but rather diffusion in the liquid aerosol. Two examples of volume-dependent reactions are:

$$HOBr + HCl(a) \longrightarrow BrCl + H_2O \qquad (35)$$

$$HOCl + HCl(a) \longrightarrow Cl_2 + H_2O \qquad (36)$$
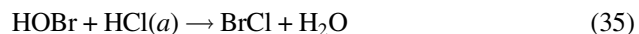
where the (a) means the species is dissolved within the aerosol. In order to calculate the rate of loss of the reactant species one needs to calculate the concentration dissolved in the aerosol. For this, the Henry's law coefficients for that gas-phase species in the solvent (usually assumed to be a binary H_2SO_4/H_2O solution) must be known. A Henry's law coefficient relates the gas-phase pressure of the species over a solution with the molality of that same species dissolved in the solution.

The rate will be given by:

$$d[\text{HOCl}]/dt = -k_{II}H_{\text{HOCl}}P_{\text{HOCl}}H_{\text{HCl}}P_{\text{HCl}}V_a \tag{37}$$

where k_{II} is the second order rate constant, H is the Henry's Law constant, P are the gas phase densities for each of the species, and V_a is the aerosol volume, typically about 1×10^{-13} cm^3 per cm^3 of air.

e *Chemical and Global Time Constants*
Ignoring dynamics, the continuity equation is given by

$$\left.\frac{dn_i}{dt}\right|_{\text{chem}} = P_i - L_i n_i. \tag{38}$$

Setting the production of the species P_i to zero, and letting the loss term L_i be constant we find the concentration

$$n_i(t) = n_i(t_0)e^{-t/\tau_{\text{chem}}} \tag{39}$$

where the chemical time constant, is defined by

$$\tau_{\text{chem}} = 1/L_i. \tag{40}$$

This gives a simple estimate of time associated with a chemical loss (or production) of any unimolecular process. In the event that the reaction is not simply an elementary reaction, the rate of the overall series of reactions is dictated by the slowest of the elementary reactions. It should be noted that the above are *local* time constants.

There is an important distinction between the local and global time constants, something which is determined by chemical reactivity and transport around the globe. A global time constant is a measure of the lifetime of a species after emission into the atmosphere. For example, at 50 km, N_2O is photolysed with a local time constant of $\sim$10 days. However, the global time constant is $\sim$120 years or more because N_2O is not very reactive in the troposphere or lower stratosphere. The lifetime then is determined by the vertical transport of N_2O from the troposphere to the upper stratosphere and stratopause, where it is readily destroyed.

4 Gas Phase Chemistry
In this section we will first look at simple oxygen chemistry, and then introduce the concept of chemical families of species, and the lifetimes associated with these families.

The formation of the stratospheric ozone layer was first described quantitatively by Chapman (1930). It can be understood on the basis of four elementary processes which are presented below. Firstly, production of $O(^3P)$, usually designated simply as O, proceeds via photolysis
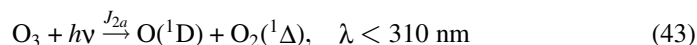
$$O_2 + h\nu \xrightarrow{J_1} 2O, \quad \lambda < 250 \text{ nm.} \tag{41}$$
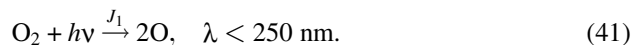
Secondly, the O atoms produced in this manner rapidly form ozone (e.g., in $\sim$5 milliseconds at 30 km)

$$O + O_2 + M \xrightarrow{k_1} O_3 + M. \tag{42}$$

Thirdly, the product ozone which can photolyse quite quickly ($<$100 s to $\sim$ 1 hour depending on the height) to give $O(^1D)$ and $O(^3P)$ as well as molecular oxygen in two different quantum states depending on the energy of the impinging photon:

$$O_3 + h\nu \xrightarrow{J_{2a}} O(^1D) + O_2(^1\Delta), \quad \lambda < 310 \text{ nm} \tag{43}$$

$$\xrightarrow{J_{2b}} O(^3P) + O_2(^3\Sigma). \tag{44}$$

Since ozone production is driven by solar radiation, the maximum ozone production rate is over the tropics at about 40 km. However, the loss is likewise large at these altitudes so that the peak in the ozone actually occurs at lower altitudes. The $O(^1D)$ is rapidly ($\sim$10 ns at 30 km) quenched to $O(^3P)$ releasing the 1.9 eV as kinetic energy. The O formed, rapidly reforms ozone with the result that most of the energy absorbed by O_3 is released locally as kinetic energy. At altitudes above $\sim$60 km, where M is about 1% or less than that at 30 km, some of the 1.9 eV from the $O(^1D)$ is lost directly as IR radiation from electronically excited O_2 without contributing to a temperature increase (Mlynczak and Solomon, 1993).

$$O(^1D) + M \xrightarrow{k_2} O + M + K_e \tag{45}$$

$$\text{Net}: \ h\nu \rightarrow \text{heating.} \tag{46}$$

Finally, ozone can be lost by

$$O + O_3 \xrightarrow{k_3} 2O_2. \tag{47}$$

Given the above processes, the local continuity equations for O and O_3 are given by

$$\frac{d[O]}{dt} = 2J_1[O_2] + J_{2b}[O_3] + k_2[O(^1D)][M] - [O]\{k_1[O_2][M] + k_3[O_3]\} \tag{48}$$

$$\frac{d[O(^1D)]}{dt} = J_{2a}[O_3] - k_2[O(^1D)][M] \tag{49}$$

$$\frac{d[O_3]}{dt} = k_1[O][O_2][M] - [O_3](J_{2a} + J_{2b} + k_3[O]). \tag{50}$$

Since there is a rapid interchange between, $O_x = O + O(^1D) + O_3$, the sum of these species is identified as O_x and called the odd oxygen family, viz.,

$$O_x = O + O(^1D) + O_3. \tag{51}$$

The equation describing the chemical behaviour of the O_x family as a unit may be written

$$\frac{d[O_x]}{dt} = 2J_1[O_2] - 2k_3[O][O_3]. \tag{52}$$

This clearly identifies the sole origin of the ozone, namely, photolysis of O_2. Likewise, in this simplified chemical scheme, the sole loss is due to reaction (47).

There are various chemical time constants associated with each of these species. The lifetimes of the individual species constituting the O_x family will vary with altitude and the local chemical environment but lifetimes for each can be approximated for typical stratospheric conditions at 30 km (Brasseur and Solomon, 1986):

$$\tau_{O_3} = \frac{1}{J_2 + k_3[O]} \sim \frac{1}{J_2} \sim 2000 \text{ s} \tag{53}$$

$$\tau_O = \frac{1}{k_1[O_2][M] + k_3[O_3]} \sim \frac{1}{k_1[O_2][M]} \sim 0.04 \text{ s} \tag{54}$$

where we have dropped the small terms in the denominators. From equation (52) we can write the time constant for odd oxygen, O_x as

$$\tau_{\text{chem}}^{O_x} = \frac{O + O_3}{2k_3[O][O_3]}. \tag{55}$$

For altitudes less than 60 km, $O \ll O_3$, hence $\tau_{\text{chem}} = \frac{1}{2k_3(O)} \sim 5$ days at about 50 km. Note that it is inversely proportional to O densities which decrease (super) exponentially as pressure increases.

To generalize from oxygen chemistry, ozone can also be lost by reactions with many other species. A molecule can react in a sequence of elementary processes to eliminate O, O_3 or both (producing O_2) but not be consumed itself in the reaction because the molecule(s) is/are continually being regenerated within the *catalytic cycle*. Some catalytic cycles are quite complicated and can involve more than one chemical family (e.g., Lary, 1997).

In the following sections we will briefly introduce the various catalytic cycles involved in the stratosphere., We also note that, as outlined above $O_x = O_3$ below 60 km, and the destruction process is often limited by the availability of O atoms.

a *The* HO_x *Cycle*
HO_x refers to the family of free radicals which include H, OH, HO_2 and H_2O_2. HO_x is produced predominantly by reactions between water or methane and electroni-

cally excited oxygen atoms generated by the photodissociation of ozone. The reaction of water vapour and methane with $O(^1D)$ atoms is an important source of hydroxyl radicals (OH) in the stratosphere,

$$O(^1D) + H_2O \rightarrow 2OH \tag{56}$$

$$O(^1D) + CH_4 \rightarrow OH + CH_3 \tag{57}$$
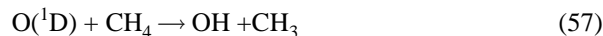
although photolysis of HOBr can also be important under conditions where its generation is high (see Section 5a). The emission sources for methane are both anthropogenic and natural: important sources are enteric fermentation, emissions from rice paddies, landfill and domestic sewage. Also, much of it comes from fossil-fuel related sources. The primary sink for methane is the reaction with tropospheric OH radicals.

In the lower stratosphere, the reactions of OH and HO_2 with ozone form an important catalytic cycle for the destruction of O_3, via

$$OH + O_3 \rightarrow HO_2 + O_2 \tag{58}$$

$$HO_2 + O_3 \rightarrow OH + 2O_2 \tag{59}$$

$$Net : 2O_3 \rightarrow 3O_2. \tag{60}$$

It is important to note that this is a catalytic cycle which is not limited by the low atomic oxygen concentrations found in the stratosphere. In the upper stratosphere, because of a large increase in atomic hydrogen concentrations, reactions such as

$$H + O_3 \rightarrow OH + O_2 \tag{61}$$

$$OH + O \rightarrow H + O_2 \tag{62}$$

$$Net : O + O_3 \rightarrow 2O_2 \tag{63}$$

become important for the destruction of ozone. In general, for background aerosol loading, HO_x is the dominant ozone-destroying family in the upper troposphere and lower stratosphere and also at altitudes greater than about 38 km (Slusser et al., 1997). However, modelling studies have shown that when processing on cirrus clouds is included, halogen-catalyzed ozone destruction may become more important near the tropopause (Solomon et al., 1997). Figure 3 shows the chemical cycling which occurs between H_2O_2, HO_2, OH and H in the stratosphere.

b *The* NO_x *Cycle*
$NO_x = NO + NO_2$ is important for O_3 loss and indeed is responsible for most of the ozone loss between about 24–38 km under background sulfate aerosol loading (Jucks et al., 1996; Slusser et al., 1997). The important sources of NO_x in the atmosphere are combustion of fossil fuels, lightning and biological activity. Approximately 90% of the green-house gas N_2O is destroyed by photodissociation in the mid- to upper stratosphere to form N_2 while the remaining 10% is destroyed by $O(^1D)$ to produce two NO molecules. The emission of NO_x from combustion results
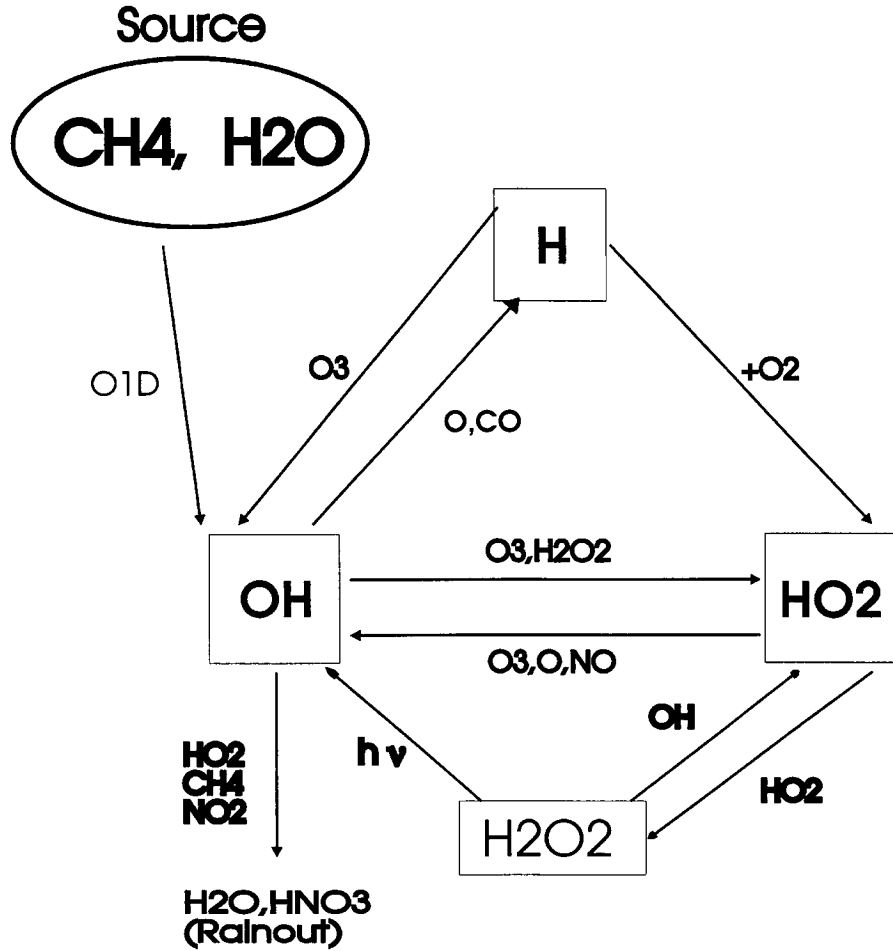
Source

Fig. 3   Nicolet diagram for the HO_x family.

from both fossil fuel usage and biomass burning. During the winter season, NO_x is injected into the stratosphere by downwelling from the ionosphere, where it is produced by the dissociation of molecular nitrogen by solar UV and auroral electrons. Finally, NO_x can be produced by cosmic rays in the stratosphere and by lightning in the upper troposphere which can then become a source of stratospheric NO_x by tropical upwelling.

The main O_3 loss cycle is

$$NO_2 + O \rightarrow NO + O_2 \tag{64}$$

$$NO + O_3 \rightarrow NO_2 + O_2 \tag{65}$$

$$\text{Net}: O + O_3 \longrightarrow 2O_2. \tag{66}$$
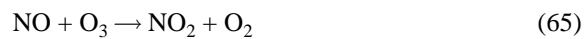
The rate of ozone destruction by this cycle is limited by the low abundance of O and thus the rate limiting step is the $O + NO_2$ reaction. When this reaction occurs, reaction (65) occurs ~100% of the time and therefore the ozone loss rate for this cycle can be written approximately as $2k_{64}[NO]_2[O]$. The following scheme

$$NO + O_3 \longrightarrow NO_2 + O_2 \tag{67}$$

$$NO_2 + h\nu \longrightarrow NO + O \tag{68}$$

$$O + O_2 + M \longrightarrow O_3 + M \tag{69}$$

$$\text{Net}: h\nu \longrightarrow \text{heating} \tag{70}$$

does not result in **net** O_3 loss. Rather it leads to heating of the stratosphere.

Recent studies show that under volcanically perturbed conditions, such as that which occurred after the eruption of Mount Pinatubo, large ambient amounts of sulfate aerosol cause a large-scale conversion of NO_x to the (relatively) chemically inert HNO_3 (Section 4d) while increasing the concentration of HO_x and of halogens (see Section 5). This conversion decreases the amount of ozone destruction through the NO_x catalytic cycles but increases the amount of destruction from both the HO_x and the ClO_x family (e.g., Zhao et al., 1997). It is also important to note that ozone loss after a large volcanic eruption is a strong function of the amount of inorganic chlorine available in the stratosphere (Brasseur et al., 1997). It was shown in that study that ozone levels can even increase in regions (above 22 km) of the Antarctic vortex under pre-industrial chlorine loading levels (~0.6 ppbv).
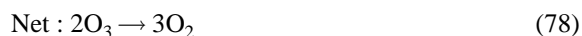
c *Halogen Cycles*
Important source gases for stratospheric chlorine are methyl chloride (~20%) which has a natural origin and chlorofluoromethanes (CFCs; ~80%) etc. which have anthropogenic sources. The photolysis of the halocarbons leads to the generation of atomic chlorine and ClO in the stratosphere. Atomic bromine is created through the photolysis of halons transported from the troposphere and through the destruction of CH_3Br. Although the mixing ratio of bromine is small, it can contribute, as much as 30% of the total ozone loss during formation of the austral ozone hole (e.g., de Grandpré et al., 1997). Interaction with ozone results in catalytic cycles such as

$$X + O_3 \longrightarrow XO + O_2 \tag{71}$$

$$XO + O \longrightarrow X + O_2 \tag{72}$$

$$\text{Net}: O + O_3 \longrightarrow 2O_2 \tag{73}$$

or the sequence

$$X + O_3 \longrightarrow XO + O_2 \tag{74}$$

$$Y + O_3 \longrightarrow YO + O_2 \tag{75}$$

$$XO + YO \longrightarrow XY + O_2 \tag{76}$$

$$XY + h\nu \longrightarrow X + Y \tag{77}$$
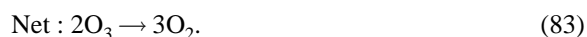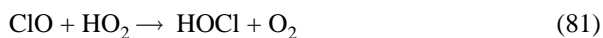
$$\text{Net}: 2O_3 \longrightarrow 3O_2 \tag{78}$$

where X = Cl or Br atoms. The former sequence is again limited by the low abundance of O atoms but the latter is not. An example of the latter sequence involves the ClO dimer (both X and Y = Cl above) which can destroy ozone with a rate proportional to the square of the ClO concentration (see Section 5b).
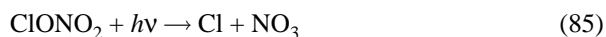
Fluorine molecules can also be produced as a result of the dissociation of CFCs. However, F atoms and FO molecules are effectively stabilized as HF. The HF molecule does not react appreciably with the OH radical (in contrast to HCl + OH $\rightarrow$ Cl + H$_2$O) and as such the stratospheric concentrations of free F and FO are quite small and their effect on odd oxygen chemistry is insignificant (Brasseur and Solomon, 1986). Iodine, although quite chemically active, is also not important because of the very low concentration.

An interaction also occurs between the chlorine and HO$_x$ families where ClO reacts with HO$_2$ to form hypochlorous acid (HOCl) which leads to ozone loss:

$$HOCl + h\nu \longrightarrow OH + Cl \tag{79}$$

$$Cl + O_3 \longrightarrow ClO + O_2 \tag{80}$$

$$ClO + HO_2 \longrightarrow HOCl + O_2 \tag{81}$$

$$OH + O_3 \longrightarrow HO_2 + O_2 \tag{82}$$

$$\text{Net}: 2O_3 \longrightarrow 3O_2. \tag{83}$$

The rate limiting step in this sequence is the photolysis of hypochlorous acid. Consequently, this cycle is not important when the sun is down but is important in the sunlit polar lower stratosphere (Lary, 1997).

Similarly, an important coupling of the ClO$_x$ and NO$_x$ families occurs through the following cycle:

$$ClO + NO_2 \longrightarrow ClONO_2 \tag{84}$$

$$ClONO_2 + h\nu \longrightarrow Cl + NO_3 \tag{85}$$

$$NO_3 + h\nu \longrightarrow NO + O_2 \tag{86}$$

$$NO + O_3 \longrightarrow NO_2 + O_2 \tag{87}$$

$$Cl + O_3 \longrightarrow ClO + O_2 \tag{88}$$

$$\text{Net}: 2O_3 \longrightarrow 3O_2. \tag{89}$$

This sequence is most important at mid-latitudes and at approximately 20 km altitude. The rate limiting step is the ClONO$_2$ photolysis except in the upper stratosphere where the production of ClONO$_2$ is rate limiting (Lary, 1997).

d *Reservoirs*

Many chemical species exist which do not readily attack ozone. For example, the reaction between OH and NO_2, both of which are actively involved in the destruction of ozone,
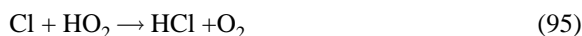
$$OH + NO_2 \rightarrow HNO_3 \tag{90}$$

produces HNO_3 which is inert towards ozone. In the lower stratosphere, this can prevent the reaction of much of the nitrogen, $NO_y = NO_x + HNO_3 + HNO_2 + ...$ which means that there is less NO_x available to attack ozone. Species such as these are called **reservoir species** since they act as temporary storage locations for the more active forms of nitrogen. It should be noted here that there is a dynamic equilibrium between reservoir and active forms within a chemical family, and there are many factors affecting their relative concentrations (radiation, heterogeneous processing, temperature etc.) The HNO_3 can be converted to NO_x by photolysis or reaction with OH

$$HNO_3 + h\nu \rightarrow OH + NO_2 \tag{91}$$

$$HNO_3 + OH \rightarrow H_2O + NO_3 \tag{92}$$
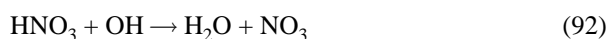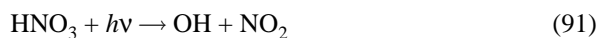
with a time constant of a few days to 2 weeks depending on altitude and season. Figure 4 shows the nitrogen Nicolet diagram and how the main reservoir species, HNO_3, $ClONO_2$ and N_2O_5 play a major role. The HNO_3 reservoir is most important in the lower stratosphere below 30 km and can represent up to 90% of the NO_y. Figure 4 also indicates that transport to the troposphere and subsequent wet deposition and rain out is the ultimate sink for the NO_x.

The main chlorine reservoir species are HCl and $ClONO_2$ formed by

$$Cl + CH_4 \rightarrow HCl + CH_3 \tag{93}$$

$$Cl + HCHO \rightarrow HCl + CHO \tag{94}$$

$$Cl + HO_2 \rightarrow HCl + O_2 \tag{95}$$

and

$$ClO + NO_2 + M \rightarrow ClONO_2 + M \tag{96}$$
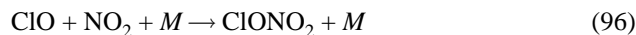
respectively. Figure 5 summarizes the Cl_y chemistry while Figs 6a and 6b show the amount of Cl present as HCl and $ClONO_2$ reservoir species. Figure 6c shows the total inorganic chlorine amount as modelled in the Canadian Middle Atmosphere Model (CMAM) while Fig. 6d shows CMAM total nitrogen concentrations (ppbv). In most of the stratosphere when there is no heterogeneous conversion of reservoir species to active forms (Section 5), total chlorine is predominately in the form of HCl, approximately 3.5 ppbv in the lower stratosphere at mid-latitudes. Total nitrogen reaches a maximum of about 22 ppbv over the tropics at about 3 mb pressure (40 km). The photolysis of N_2O is the reason for this feature.
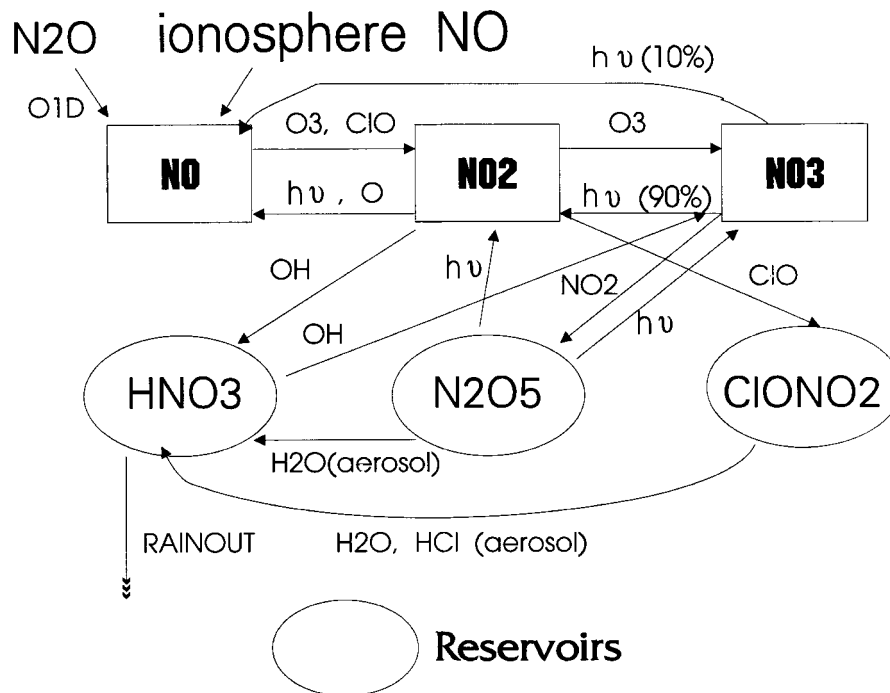
Fig. 4   Nicolet diagram for the NO_x family.

Bromine species are present in the stratosphere as well but concentrations reach only approximately 20 pptv in the mid- to upper stratosphere (Chartrand and McConnell, 1998). However, a particular amount of total bromine is much more effective at destroying ozone than is the same amount of total chlorine. This is because the bromine analogues to the chlorine reservoirs are relatively much less abundant. For example, while HCl is formed through the reaction of CH_4 with atomic chlorine, the same reaction for Br is endothermic and extremely slow. HBr then must be formed predominately through the reaction of Br with HO_2, HCHO or through the minor branch of BrO + OH (Chartrand and McConnell, 1998). Also, HBr is much more photolytic than is HCl: the photolysis constant for HCl is 2.9×10^{-9} s^{-1} while for HBr it is 2.0×10^{-7} s^{-1} for a directly overhead sun at 20 km altitude. Finally, the reaction of OH with HBr is much faster than the same reaction with HCl. The rate constant for HBr for this reaction is two orders of magnitudes faster than that for HCl (DeMore et al., 1997). All these factors lead to a chemical lifetime of HBr of only a couple of days, while for HCl, it is on the order of a month. Similarly, the $BrONO_2$ lifetime is minutes, while for $ClONO_2$, it is hours. Figure 7 gives a summary of some of the sources for each of the chemical families discussed above.

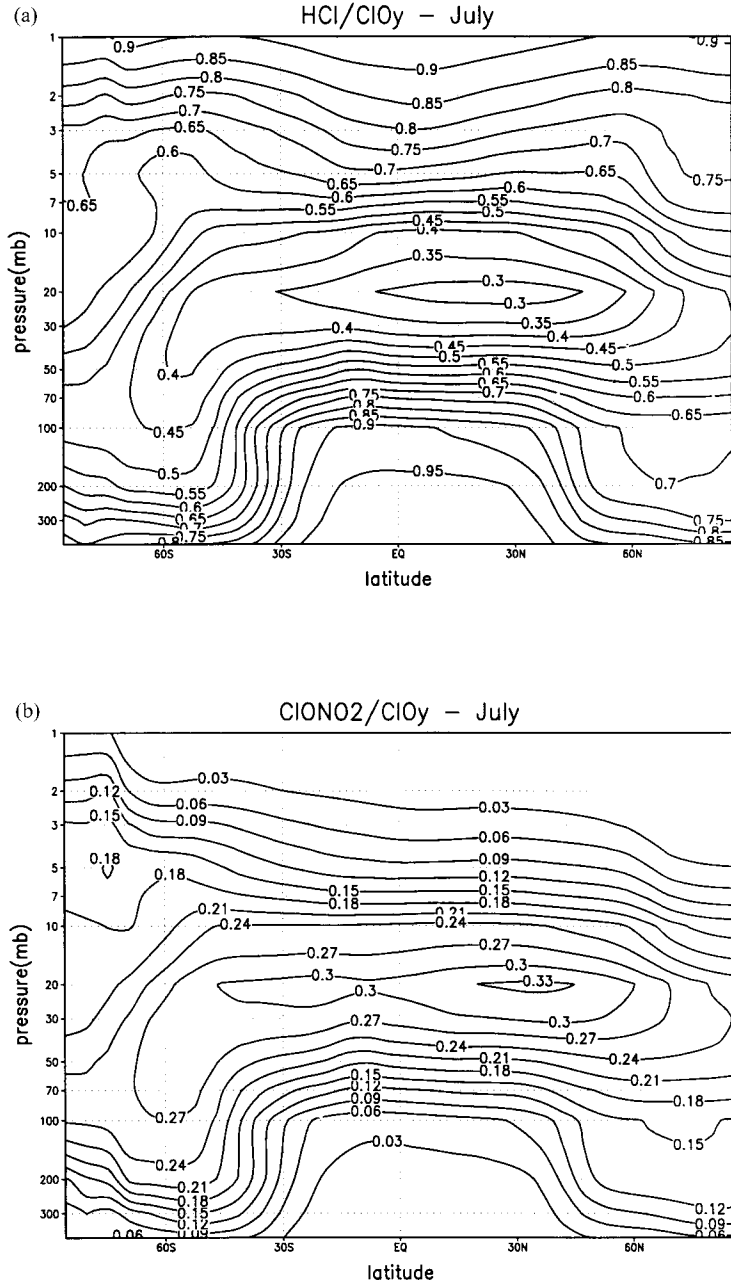Fig. 5   Nicolet diagram for the ClO_x family.

5 Heterogeneous Chemistry

Reactions which occur on/in a condensed phase such as a liquid and/or a solid are known collectively as heterogeneous reactions. Small condensation nuclei can form in the troposphere and stratosphere by homogeneous nucleation, and these nuclei in turn can grow by condensation and coagulation or by heterogeneous nucleation as discussed in Section 3c. Once formed, these aerosol particles can act as surfaces upon which reactions can proceed; reactions which are normally kinetically limited in the gas phase.

Gas phase species such as H_2O and HCl are first sequestered onto or into the aerosol. The rate of heterogenous HBr processing is generally smaller than other HBr destruction reactions. The mechanism of HCl uptake is a matter of current research but it is thought that there is a dynamic character to the aerosol surfaces: constant evaporation and condensation. Haynes et al. (1992) suggest that HCl is able to ionize on the aerosol surface by being surrounded by H_2O molecules condensing back onto the surface.

(a)

HCl/ClOy — July

(b)

ClONO2/ClOy — July

Fig. 6   Partitioning of the Cl family: (a) HCl (b) ClONO$_2$ (c) total chlorine and (d) total NO$_y$. All panels taken from the Canadian Middle Atmosphere Model (reproduced from de Grandpré et al., 1997).

(c)

ClOy — July

(d)

NOy(ppbv) — July

Fig. 6   (*Concluded*).

$$O_3 : h\nu \quad (NO + HO_2 \mathbin{-\!\!\!>} NO_2 + OH)$$
$$HO_x : H_2O, CH_4, [HOBr]$$
$$NO_x : N_2O, \text{ionosphere, oceans, agriculture}$$
$$ClO_x : \text{CFCs (80\%)}, CH_3Cl \text{ (20\%)}$$
$$BrO_x : \text{Halons, } CH_3Br \text{ (natural and anthropogenic)}$$
$$\text{aerosols} : SO_2, COS, \text{volcanos}$$
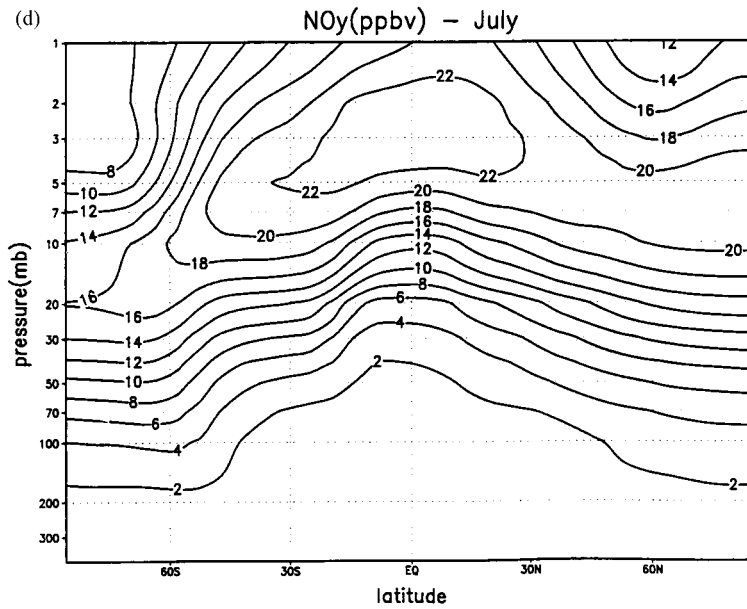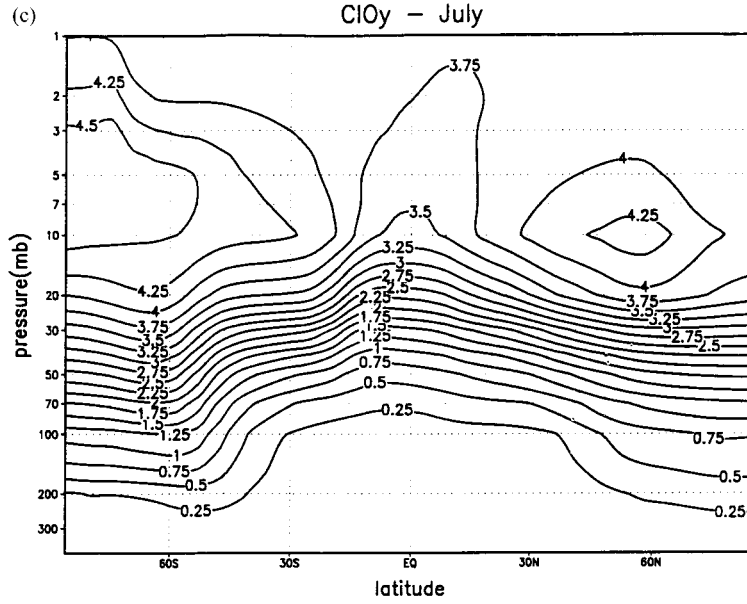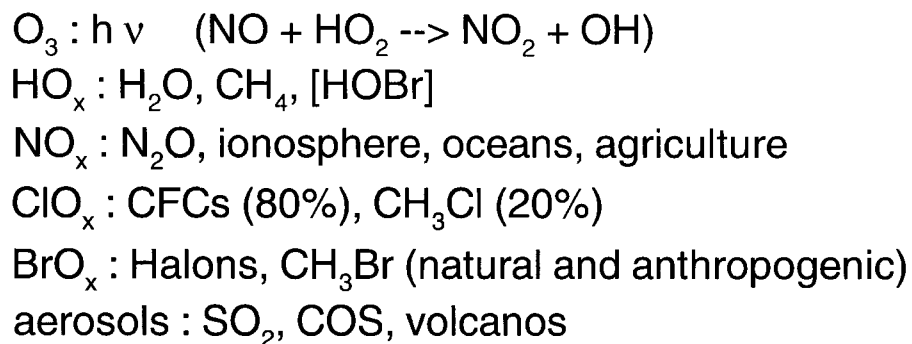
Fig. 7   A summary of the sources of many chemical families considered in stratospheric chemical models.

This mechanism means that a pseudo-liquid aerosol surface is not required in order for effective HCl uptake to occur just a dynamic ice surface (Clary, 1996). This distinction is important because modelling efforts have shown that HCl remains adsorbed on an ice surface for only about 10^{-7} seconds, not long enough for a significant number of diffusion-limited reactions to take place (Kroes and Clary, 1992). A second molecule then impinges on the aerosol surface and a subsequent reaction can take place with the previously dissolved HCl or H_2O. The rate of a reaction of this type will be dependent on surface area but it is possible that there will be significant diffusion of the adsorbed/absorbed species into the aerosol. In this case, the rate of the reaction will be proportional to the available aerosol volume (see Section 3d). Generally, there are two major types of surfaces which are considered in most atmospheric models: (1) sulfate aerosols and (2) PSCs, each of which will be considered separately below.

Heterogeneous reactions, which occur on and within sulfate aerosols, play an important role in the stratosphere. The particles are ubiquitous but the highest concentration is in the lower stratosphere (about 5 km below the peak of ozone mass density) as determined by numerous experiments such as SAM I (Stratospheric aerosol measurement), SAM II and SAGE (Stratospheric Aerosol and Gas Experiment; e.g., McCormick, 1987; Thomason et al., 1997b). The main aerosol layer at ~20 km consists of sulfate aerosols which, at mid-latitudes, have a weight composition of about 75% H_2SO_4 and 25% water (or about a 2:1 water:H_2SO_4 mole ratio). However, the composition is temperature dependent with the percentage of acid decreasing with decreasing temperature.

These particles are predominately formed by the oxidation of OCS which has a sufficiently long lifetime in the troposphere to be transported from there without being destroyed. OCS can then be photolysed in the stratosphere or react with an O atom to form SO_2 which subsequently reacts with the hydroxyl radical in the presence of a third body to form the precursor of sulfuric acid, HSO_3:
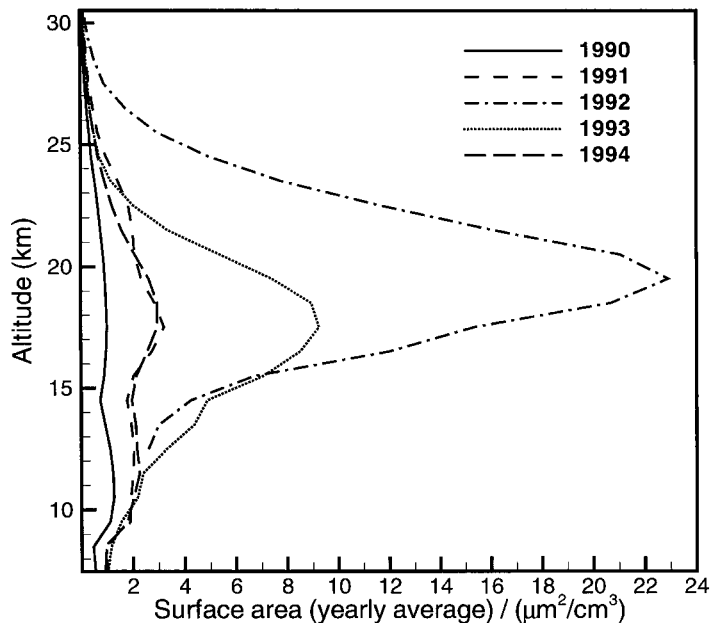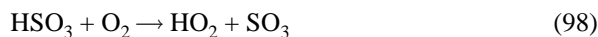
Fig. 8   The yearly averaged stratospheric aerosol surface area as determined by SAGE II measurements in the northern mid-latitudes (Thomason et al., 1997a). The years shown cover the time before, during and after the eruption of Mount Pinatubo in June 1991. "Background" aerosol surface area is approximately 0.6 μm^2 cm^{-3} at about 20 km.

$$SO_2 + OH + M \rightarrow HSO_3 \qquad\qquad (97)$$

$$HSO_3 + O_2 \rightarrow HO_2 + SO_3 \qquad\qquad (98)$$

$$SO_3 + H_2O \rightarrow H_2SO_4. \qquad\qquad (99)$$

The H_2SO_4 then nucleates with water to form aerosol particles which have a radius of about 0.1 to 0.5 μm (e.g., Dye et al., 1993). Other important sources of sulfur-containing compounds in the middle atmosphere come from random volcanic activity in the troposphere which can penetrate the tropopause. Large eruptions such as that of Mount Pinatubo in June of 1991 resulted in the deposition of between 15 to 30 megatons of SO_2 with subsequent generation of sulfate aerosol (e.g., Brasseur and Granier, 1992; Cole-Dai et al., 1997).

   Figure 8 shows the annual averaged aerosol surface areas for the 30 to 40°N latitude band as derived from the SAGE II data of Thomason et al. (1997b). Normal background conditions are seen in 1990 when surface areas are about 0.6-0.7 μm^2 cm^{-3}. However, in 1992, the large influx of volcanic SO_2 substantially increases the available surface area by a factor of 20 at around 20 km. The subsequent years show the amount of sulfate aerosol surface area returning to normal conditions.

An important question that has arisen and is still active is the extent to which anthropogenic activity has increased the mass density of sulfate aerosol in the stratosphere. Hofmann (1990) argued that a direct comparison of late 1988 sulfate aerosol mixing ratio with those from 1974 and 1979 (both periods were relatively unperturbed by volcanic effects) showed an increase of about 3.8% per annum. However, Thomason et al. (1997a) argued that the late 1980s data still contained remnants of previous volcanic activity and as such were not indicative of true "background" conditions.

The formation of a strong polar vortex in the winter stratosphere tends to isolate the polar air from the mid-latitude air, although there is some downward vertical mixing due to slow radiatively-driven circulation. The vortex forms largely as a result of the infrared cooling that occurs during the winter, which causes temperatures to drop well below 200 K. Solutions and/or solids consisting of H_2SO_4, H_2O, HNO_3 and HCl are able to form. Also, each winter and spring since 1979 a substantial decrease in the austral ozone column has been observed (Farman et al., 1985) in this vortex region leading researchers to postulate that temperature and ozone levels are correlated (Solomon et al., 1986). In general, when temperatures are above approximately 195–200 K and under 'normal' stratospheric conditions, there is little dissolved HNO_3 in the sulfate aerosols and the heterogeneous chemistry is similar to that at mid-latitudes, although some reactions may be more important due to increased solubilities (see below).

As the solution undergoes further cooling, as in a polar vortex, HNO_3 can dissolve into the sulfate aerosols to form a ternary solution in amounts large enough to almost entirely deplete gas phase HNO_3 levels. The volume of these aerosol solutions can dramatically increase by an order of magnitude or more with this large uptake of gaseous HNO_3 and H_2O. It is thought that these supercooled ternary $H_2SO_4/HNO_3/H_2O$ liquid solutions (PSC type 1b) can exist to a few degrees below the ice frost point without forming solid PSC type 1a nitric acid trihydrate ($HNO_3 \cdot 3H_2O$ or NAT), or PSC type 2 solid water ice.

Another solid surface upon which heterogeneous reactions are known to occur is sulfuric acid tetrahydrate ($H_2SO_4 \cdot 4H_2O$ or SAT). (Carslaw et al., 1994, 1995; Tabazadeh et al., 1994, 1997). Finally, there are reported cases of type 1 PSC exhibiting only moderate depolarization and other characteristics not consistent with either types 1a or 1b. These particles, inferred from the ER-2 aircraft measurements, have been classified as type 1c in the literature (Tabazadeh and Toon, 1996).

When the atmosphere cools below the water ice frost point ($\sim$188 K), type 2 PSCs made of water ice can form. Type 1 PSCs and SAT are also able to nucleate and freeze after water ice is formed. Once these solid surfaces are formed, SAT may exist up until the temperature increases to about 215 K, while NAT may exist until about 195 K, their respective melting points. However, NAT may first melt and liberate gaseous HNO_3, which can cause SAT and the gaseous HNO_3 to reform an $H_2SO_4/HNO_3/H_2O$ ternary solution at temperatures far below the normal SAT melting point (Tolbert, 1996; Koop and Carslaw, 1996). The nature of the microphysics
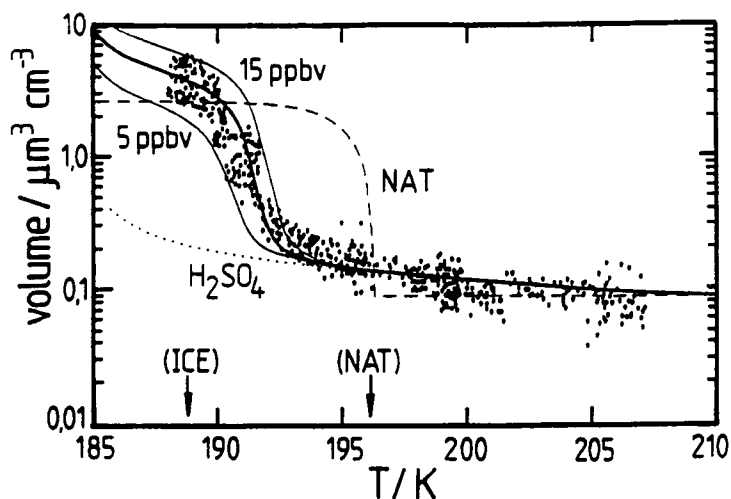
Fig. 9   A comparison of observed (Dye et al., 1992) and modelled (Carslaw et al., 1994) aerosol particles volumes using a supercooled ternary solution model. The solid lines correspond to volumes calculated using 5, 10 and 15 ppbv HNO_3 in the gas phase. The dashed line labelled nitric acid trihydrate (NAT) is the volume calculated assuming NAT deposition onto frozen aerosols. Finally, the dotted line labelled H_2SO_4 is that calculated assuming no uptake of HNO_3, only H_2O. The vertical arrows indicate the expected ice and NAT formation temperatures under standard atmospheric conditions (reproduced from Carslaw et al., 1994, copyright by the American Geophysical Union).

of this complicated system is quite important and is an active area of research (e.g., Koop et al., 1997; Peter, 1997).

The importance of when and for how long each of the solid and liquid heterogeneous surfaces appears stems from the fact that the rate of heterogeneous conversion of reservoir species can be different on one surface compared to another (DeMore et al., 1997; Sessler et al., 1996). Due to the low temperatures needed for solid PSCs to form, it is expected that processing on liquid surfaces is more important in the Arctic than in the Antarctic.

The uptake of HNO_3 and H_2O as described above is shown in Fig. 9. This figure shows a comparison between aerosol volumes calculated by Carslaw et al. (1994) using a ternary solution model and those observed by Dye et al. (1992). The curve labeled H_2SO_4 is the volume predicted assuming no uptake of nitric acid into the aerosol, only water vapour. The curve labeled NAT shows the aerosol volume expected if only NAT were formed when gas phase nitric acid concentrations become larger than the equilibrium amount over NAT at that temperature (under normal stratospheric conditions, this is about 195–196 K). Clearly, these two curves do not agree well with observed volumes, indicating that these are almost certainly not the mechanisms by which aerosols grow at temperatures near 192 K. However, agreement is very good between the curves which assume an uptake of nitric acid and water to form a ternary solution.
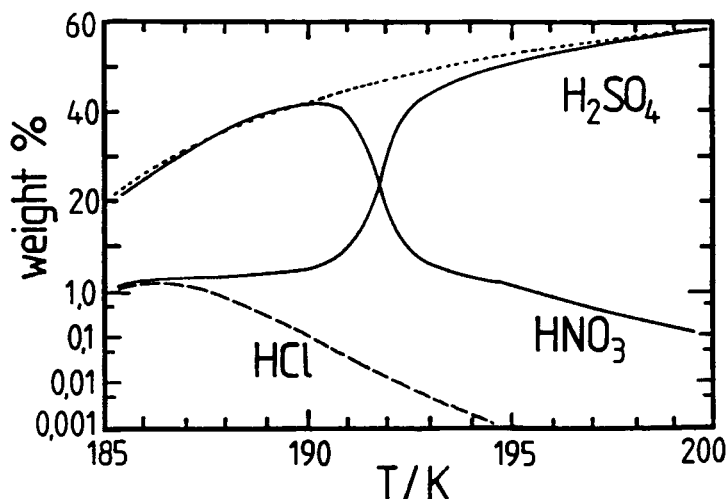
Fig. 10   The modelled composition of the H_2SO_4(0.5 ppbv)-HNO_3(10 ppbv)-HCl(1 ppbv)-H_2O(5 ppmv) liquid aerosol. The dashed dotted line shows the composition assuming no HNO_3 or HCl uptake into the liquid aerosol (reproduced from Carslaw et al., 1994, copyright by the American Geophysical Union). Note the change in scale at 1% on the y-axis.

Figure 10 shows the weight percentage composition of the aerosols as temperature decreases from 200 to 185 K. The large uptake of nitric acid is seen at about 192 K when its percentage composition rises from a few percent to about 40%. Similarly, HCl rises from being a minor component at 195 K to 1% or more near 185 K. (Note the change in scale below 1% on the ordinate.) Due to the large uptake of HCl and subsequent heterogeneous processing (see Section 5b), liquid PSCs are able to produce elevated ClO levels in non-denitrified air (WMO, 1999).

Recently, the effects of mountain-induced gravity waves on the formation of PSCs have been investigated by Carslaw et al. (1998). The waves are known to cause local reductions in temperature by as much as 10–15 K below that expected synoptically. These mesoscale PSC formations offer a possible explanation for the underprediction of reactive chlorine levels and Arctic ozone depletion in many models (Carslaw et al., 1998).

a *Sulfate Aerosol Chemistry*

Two important reactions occurring on sulfate aerosols at mid-latitudes in the lower stratosphere are

$$N_2O_5 + H_2O(a) \longrightarrow 2HNO_3 \tag{100}$$

$$BrONO_2 + H_2O(a) \longrightarrow HOBr + HNO_3 \tag{101}$$
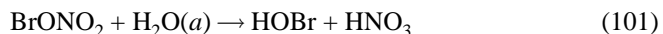
where (*a*) means that the species is in the liquid phase of the aerosol and the reaction

is a heterogeneous reaction. These hydrolysis reactions are important since they change the relative balance between active and reservoir species (e.g., Danilin and McConnell, 1995). Thus, the NO_x/NO_y ratio may decrease due to conversion of N_2O_5 and $BrONO_2$ to HNO_3. However, while the nitrogen-cycle ozone losses may decrease, ozone loss due to HO_x and ClO_x may increase. Active chlorine species will increase because the reduction in NO_2 will result in less ClO being present as $ClONO_2$, a chlorine reservoir species. Odd hydrogen will also increase due to the photolysis of HOBr and HNO_3 viz.

$$HOBr + h\nu \rightarrow OH + Br \tag{102}$$

$$HNO_3 + h\nu \rightarrow OH + NO_2. \tag{103}$$
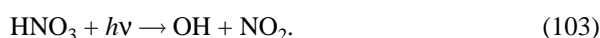
The enhanced OH and HO_2 will increase ozone destruction through the HO_x catalytic cycles (for example see Section 4a). In addition, the increased OH will also release Cl from HCl, another reservoir species through the following reaction:

$$OH + HCl \rightarrow Cl + H_2O. \tag{104}$$

The above reaction also results in increased ClO levels.

It should be noted, however, that the influence of increased sulfate aerosols on these hydrolysis reactions is subject to saturation effects. Thus, the conversion of NO_x to HNO_3 is ultimately limited by the (mostly) night-time formation of N_2O_5 via

$$NO_2 + O_3 \rightarrow NO_3 + O_2 \tag{105}$$

$$NO_2 + NO_3 + M \rightarrow N_2O_5 + M \tag{106}$$

with the former reaction being rate limiting. As for $BrONO_2$ hydrolysis, the increase in HNO_3 is limited by the increase in OH by

$$OH + HNO_3 \rightarrow H_2O + NO_3 \tag{107}$$
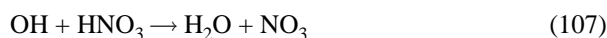
where the OH increase occurs as a result of the hydrolysis reaction. Also, during the day, $\sim$90% of the NO_3 photodissociates to form O which reduces the amount of ozone lost. About 10% of the NO_3 photodissociates to NO and O_2, with a small odd oxygen loss.

Another reaction which becomes important when the temperature decreases below about 205 K is

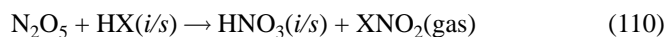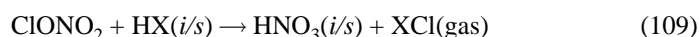$$ClONO_2 + H_2O(a) \rightarrow HOCl + HNO_3. \tag{108}$$
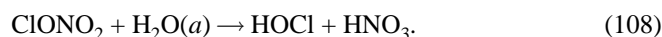
This reaction is expected to become important at higher latitudes where temperatures are generally lower or under volcanically induced conditions (Zhao et al., 1997).

b *Polar Stratospheric Cloud Chemistry*
Heterogeneous reactions on these condensed phases can activate chlorine and bromine with odd nitrogen as $HNO_3(a)$ (e.g., Tolbert, 1996). The active chlorine and, to

a lesser extent, bromine drive the reactions that form the ozone hole. For example, on the ice crystals, inactive or reservoir forms of the halogen catalysts are freed through the following reactions

$$ClONO_2 + HX(i/s) \rightarrow HNO_3(i/s) + XCl(gas) \tag{109}$$

$$N_2O_5 + HX(i/s) \rightarrow HNO_3(i/s) + XNO_2(gas) \tag{110}$$

where (i/s) means the species remains in/on the ice surface or dissolved within the aerosol solution and where X = Cl, Br.

Low temperatures are crucial to this process. As the polar lower stratospheric temperatures decrease at the end of the fall season, these PSC reactions become important. For example, the solubility of HCl is very temperature dependent, and as the temperature drops, HCl begins to dissolve in the ternary solution or sulfate aerosol as seen in Fig. 10. These and similar reactions initiate the large decrease in ozone in late polar winter (Northern Hemisphere) and austral springtime.

These reactions can occur during the night-time and, when polar sunrise occurs, species such as Cl_2, BrCl and $ClNO_2$ are readily photolysed into species such as Cl and ClO which then can participate in ozone-destroying catalytic cycles. In the austral vortex, ClO concentrations after polar sunrise can reach about 1 ppbv or more, two orders of magnitude larger than those typically found in the mid-latitude stratosphere (Anderson et al., 1991).

One of the main features of ozone loss in polar regions is that it is **not** rate limited by the low abundance of atomic oxygen. One of the main loss mechanisms involves self-reaction of ClO (Molina and Molina, 1987)
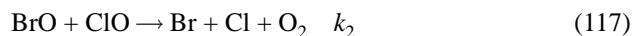
$$ClO + ClO + M \rightarrow Cl_2O_2 + M \quad k_1 \tag{111}$$

$$Cl_2O_2 + h\nu \rightarrow Cl + ClO_2 \tag{112}$$

$$ClO_2 + M \rightarrow Cl + O_2 + M \tag{113}$$

$$2 \times (Cl + O_2 \rightarrow ClO + O_2) \tag{114}$$

$$net : O_3 + O_3 \rightarrow 3O_2. \tag{115}$$

In this case the ozone loss rate is proportional to $[ClO]^2$. Thus as more ClO_y is converted to ClO, the rate of ozone destruction is quadratic with respect to active ClO_x. If temperatures are less than $\sim$210 K, then thermal decomposition of Cl_2O_2,
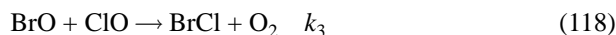
$$Cl_2O_2 + M \rightarrow ClO + ClO + M \tag{116}$$

which does not lead to ozone loss, does not play a major role.

Another important ozone loss mechanism is due to the synergistic reaction between BrO and ClO (Clyne and Watson, 1977; Yung et al., 1980):

$$BrO + ClO \rightarrow Br + Cl + O_2 \quad k_2 \tag{117}$$

$$BrO + ClO \longrightarrow BrCl + O_2 \quad k_3 \tag{118}$$

$$BrCl + h\nu \longrightarrow Br + Cl \tag{119}$$

$$Cl + O_3 \longrightarrow ClO + O_2 \tag{120}$$

$$Br + O_3 \longrightarrow BrO + O_2 \tag{121}$$

As before, this loss rate is not limited by the abundance of atomic oxygen. A major product of the reaction between BrO and ClO is OClO which in fact leads to a null cycle (no odd oxygen is destroyed). This is because OClO in the presence of sunlight rapidly dissociates to ClO and O (odd oxygen). At 190 K, approximately 60% of BrO and ClO reactions result in a null cycle, while approximately 36% form Br and ClOO (which photolyses to Cl and O_2). The remaining $\sim$4% forms the BrCl molecule (which is photolytic) and molecular oxygen.

Ozone loss rates after polar sunrise can be estimated by assuming the above two mechanisms are responsible for virtually all the O_3 destruction, then:

$$\frac{d[O_3]}{dt} = -2[ClO](k_1[ClO]+[BrO](k_2 + k_3)). \tag{122}$$

Using typical values for each of the parameters on the right (for a temperature of about 190 K):

$$[ClO] = 1.0 \text{ ppbv}$$

$$[BrO] = 8 \text{ pptv}$$

$$k_1 = 1.5 \times 10^{-13}$$

$$k_2 = 9.2 \times 10^{-12}$$

$$k_3 = 1.4 \times 10^{-12}$$

$$\text{total density} = 2.0 \times 10^{18}$$

the rate of ozone destruction can be calculated to be about three weeks for total ozone depletion. The $[ClO]^2$ term is about twice as large as the combined [BrO][ClO] term.

6 Modelling and Measurements

6.1 *Review of Models*

Modelling helps one to understand the nature of the atmosphere and allows one to forecast the effect of changes in external forcings such as solar variability, volcanic emissions, aircraft emissions, or the addition of greenhouse gases. There are various types of models, ranging from box (0-dimensional) to three-dimensional (3D), each of which offers different insights into the chemistry and physics of the atmosphere.

Box models are just that: one looks at a box or parcel of air and investigates the influence of sunlight, although one can also examine the effects of varying tempera-

ture, heterogeneous reactions, gas phase rate constants and so forth. They are used principally for analysing chemistry in the atmosphere, particularly on timescales of less than a day. They can be used either at a single point or in a trajectory mode where the box or air parcel is transported (usually unmixed) by the wind system. One of the most powerful aspects of box models is that they permit chemistry to be studied without the complicating (but real life) details of dynamics.

Box models have been used very effectively in connection with the Stratospheric Photochemistry, Aerosols and Dynamics Expedition (SPADE), Airborne Southern Hemisphere Ozone Experiment/Measurements for Assessing the Effect of Stratospheric Aircraft (ASHOE/MAESA) and Stratospheric Tracers of Atmospheric Transport (STRAT) experiments. These experiments make use of a comprehensive suite of instruments on board an ER-2 flying at an altitude of about 20 km in the stratosphere. Some of the data from the SPADE flights are shown in Fig. 11 (Salawitch et al., 1994). The data points show measurements of a number of constraining species. The solid lines in the figure are the modelled values obtained by following the air parcel at that location back several days using objectively analysed winds.

As can be seen from this figure, the current quality of the measurements is such that disagreement greater than $\sim$20% can be a cause for concern that the existing chemistry model is incorrect. One particular example is that of OH, which is shown in the first panel of Fig. 11. The disagreement between the measurements and model output at sunrise pointed to the need for a readily photolytic source of OH. This turned out to be HOBr which is produced by the heterogeneous processing of $BrONO_2$ during the night in the sulfate particles omnipresent at ER-2 altitudes (Lary, 1996): (see Eq. 103). The HOBr accumulated during the night then photolyses at sunrise, releasing a burst of OH.

Another example of the importance of box models is their application to the analysis of ATMOS (Atmospheric Trace Molecule Spectroscopy) data from the Space Shuttle (Michelsen et al., 1996). These observations have indicated that our knowledge of the partitioning of chlorine is incomplete (Fig. 12) and that other chemical reactions are required to understand the data. Because the partitioning at mid-latitudes takes place over several weeks and conditions within the air parcels are believed to be relatively uniform, a box model can be used, with some assurance, to study the relevant processes. Since the amount of active chlorine stored in reservoirs is important, the results of these analyses will have a significant influence on our understanding of the role of chlorine in the ozone chemical budget.

One-dimensional (in height) chemical diffusion models represent the atmosphere as a series of boxes stacked vertically and connected by vertical diffusion processes. In the past, these have proved very useful for preliminary and exploratory estimates of atmospheric chemistry, since much more chemistry could be incorporated in these models than in more complex models which had to account for a wider array of physical processes. However, it has become clear that the atmosphere is too complex to be understood simply in terms of a vertically connected column. In addition, computer power has burgeoned over the past 10 years to the point where chemistry
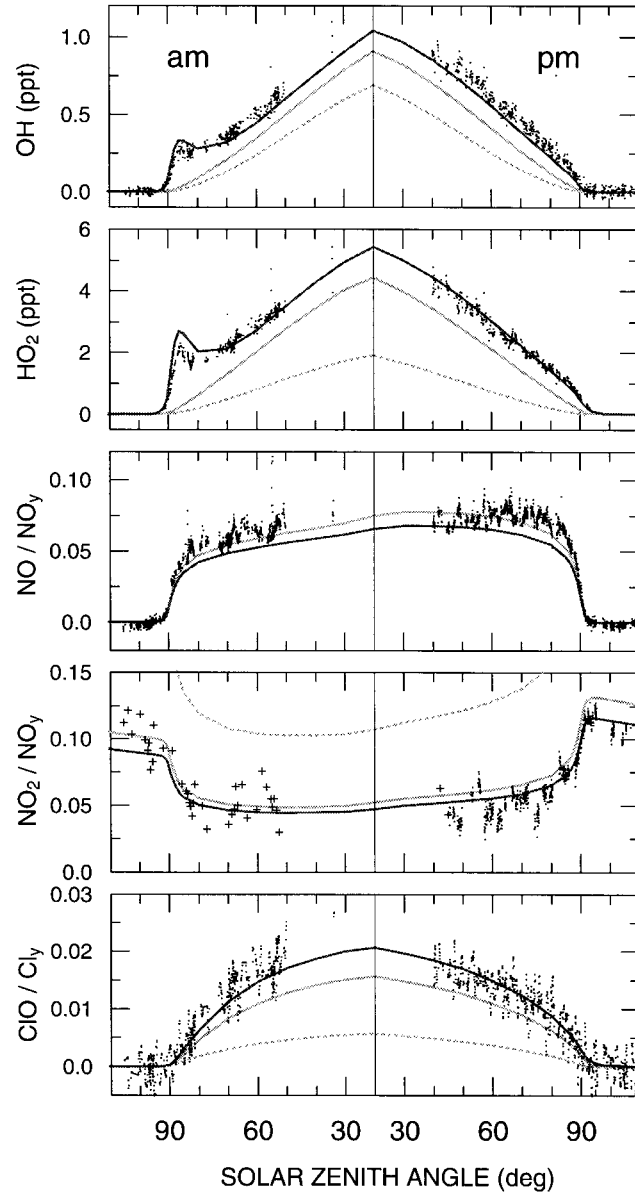
Fig. 11   Diurnal variations of OH, HO_2, NO/NO_y, NO_2/NO_y and ClO/Cl_y shown as a function of solar zenith angle. The measurements are from JPL (crosses) and NOAA (dots) instruments aboard two ER-2 flights near 37°N and 63 mb in mid-May, 1993. The dotted curves are modelled results using only gas phase chemistry, the upper solid curve in the OH, HO_2 and ClO/Cl_y panels includes the heterogeneous hydrolysis of N_2O_5 and $ClONO_2$ and a refined HNO_3 photolysis cross section (reproduced from Salawitch et al., 1994, copyright by the American Geophysical Union).
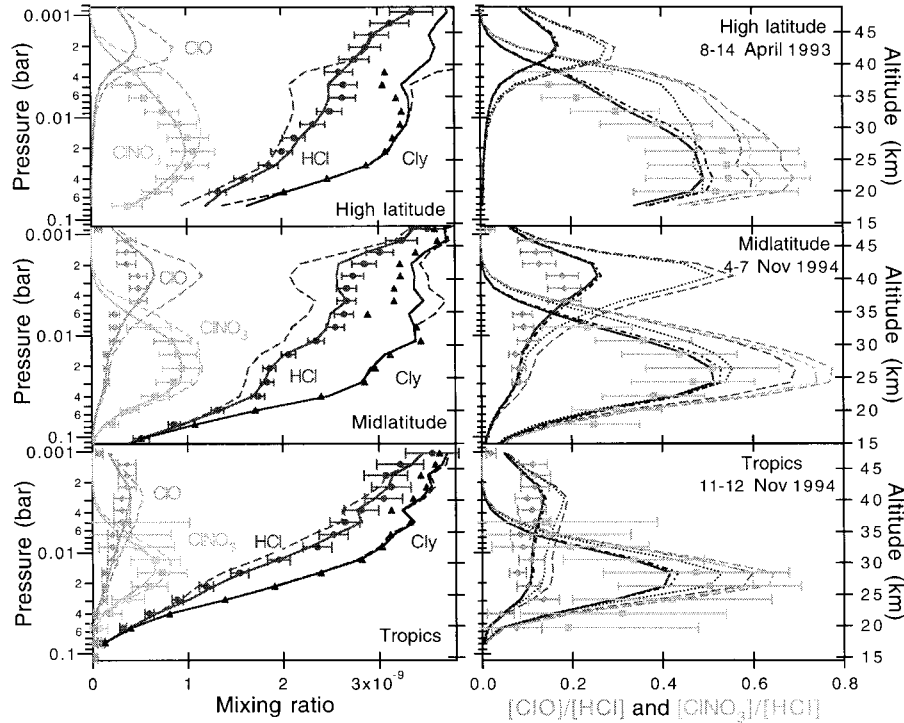
Fig. 12 A comparison of modelled and measured ClONO$_2$, HCl, Cl$_y$ (estimated) and ClO mixing ratios and ClO/HCl and ClONO$_2$/HCl concentration ratios. Model results are represented by lines, actual measurements as symbols. The vertical axis is pressure; approximate altitude is also shown. Model cases are for a variety of rates, including the standard case as described in Michelsen et al. (1996). The top panel shows concentrations at sunrise while the lower two panels are at sunset (reproduced from Michelsen et al., 1996, copyright by the American Geophysical Union).

that was once tractable only in a box or 1D model can readily be carried by higher dimensional models.

The next level of complexity in models is represented by 2D (spatial dimension) models, in which the two spatial dimensions can be either height and latitude or height and a horizontal plane. The former models (i.e., height and latitude) carry more dynamical information than 1D models but are still limited by the lack of longitudinal (zonal) variation. However, they can be readily run for much longer periods than current 3D models and so scenarios encompassing time periods of hundreds of years (the timescale of climate change) can be more readily investigated (e.g., see Tie et al., 1994 for one such model). The motivation for constructing 2-dimensional models is that some meteorological quantities are not expected to show much variation when they are averaged over a number of weeks, and the latitudinal gradient should be much larger than that in the zonal direction (Wayne, 1985).

Horizontal models in 2D using surfaces (usually potential temperature surfaces) that approximate the motion of air parcels on a timescale of a few weeks have proven very important in understanding the detailed development of the filamentary structures and their influence on atmospheric chemistry. New studies performed at very high spatial resolution (Edouard et al., 1996; Chipperfield et al., 1997) for Arctic ozone depletion, for example, have underlined the uncertainty in the modelling of ozone depletion that arises as a result of scale-dependent diffusion. A major advantage of these models is that they allow investigation of chemical and dynamical processes on scales not yet accessible by more complex models. These models are particularly useful in studying long lived tracers; species which have chemical lifetimes on the order of months or years.

With the increase in computational power, three dimensional (3D) models will be a very important tool for future work. At the present time, 3D models with full chemistry can be used to investigate long-term scenarios that even 10 years ago or less were at the limit of feasibility of 2D models. Various types of 3D models can be distinguished. There are 3D chemical transport models (CTMs) that solve the continuity equation for many chemical species: thus the species can be transported by wind fields and allowed to interact with each other. The wind fields and other meteorological data that are used can be derived from weather forecast models or atmospheric general circulation models (AGCMs). However, chemical changes in these models do not feed back on dynamics and transport or heating. These models are therefore said to be "off-line".

AGCMs are 3D models that extend from the surface to the middle atmosphere and higher and have a detailed representation of physical and dynamical processes but limited horizontal resolution (~300–500 km). These models can now incorporate interactive chemistry (chemical changes to species such as O_3 and H_2O are fed back to dynamic, transport and heating), and are used to understand and explore the terrestrial climate and its response to perturbations, both natural and anthropogenic. Weather forecast models are much like AGCMs but are run at much higher horizontal resolutions (~50–100 km) in order to resolve detailed weather patterns. They are usually used to simulate (forecast) the weather on timescales of a few days. These forecast models require the periodic input of measured data. This introduction of external information is known as *data assimilation*. Interactive chemistry has also been added to these models in order to investigate the effect of stratospheric ozone on long-range forecasting and to attempt to improve the forecasting of ozone loss over the Arctic (e.g., Kaminski et al., 1999).

Figures 13 and 14 indicate the extent to which modern models (CMAM) and observation can be compared. Figure 13 presents Cryogenic Limb Array Etalon Spectrometer (CLAES) observed (Panel a) and modelled (Panel b) CH_4 while Fig. 14 shows ISAMS observed CO (Panel a) and CMAM CO (cf. de Grandpré et al., 1997; Lopez-Valverde et al., 1996). The current version of the model is reasonably successful for each of these species. The daytime distribution of CO for June (Fig. 14) in the stratosphere and mesosphere illustrates the downward motion in the
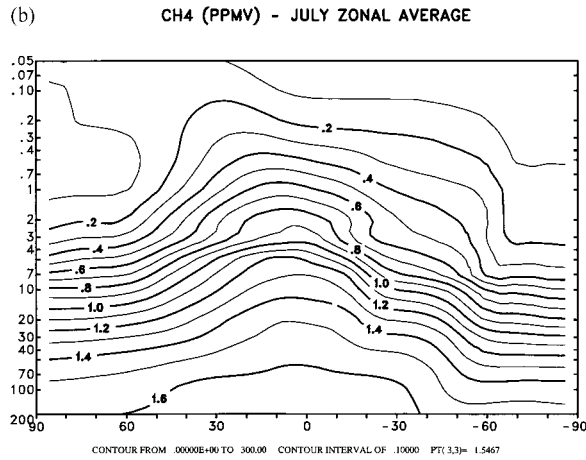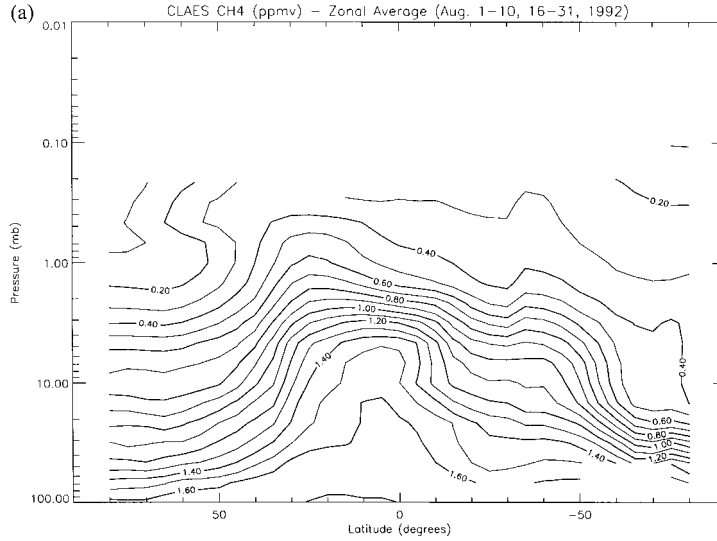
(a)

CLAES CH4 (ppmv) — Zonal Average (Aug. 1–10, 16–31, 1992)

(b)

CH4 (PPMV) - JULY ZONAL AVERAGE

CONTOUR FROM .00000E+00 TO 300.00   CONTOUR INTERVAL OF .10000   PT(3,3)= 1.5467

Fig. 13   (a) CLAES August 1992 zonal mean cross-section of CH_4 mixing ratios (ppmv) (b) July zonal average of CH_4 from CMAM, also in ppmv.

winter polar vortex region which is in quite good agreement with the Upper Atmosphere Research Satellite (UARS) CO measurements of Lopez-Valverde et al. (1996). Measurements of tracers such as CO, which are diagnostic of tropospheric air, suggest that the lowest few kilometres of the stratosphere can be affected by air convected upwards from the lower troposphere (Holton et al., 1995; Lelieveld et al.,

(a)

ISAMS CO (ppbv) — Zonal Average (June 1–2, 1992) (Daytime)

Carbon Monoxide(ppbv)
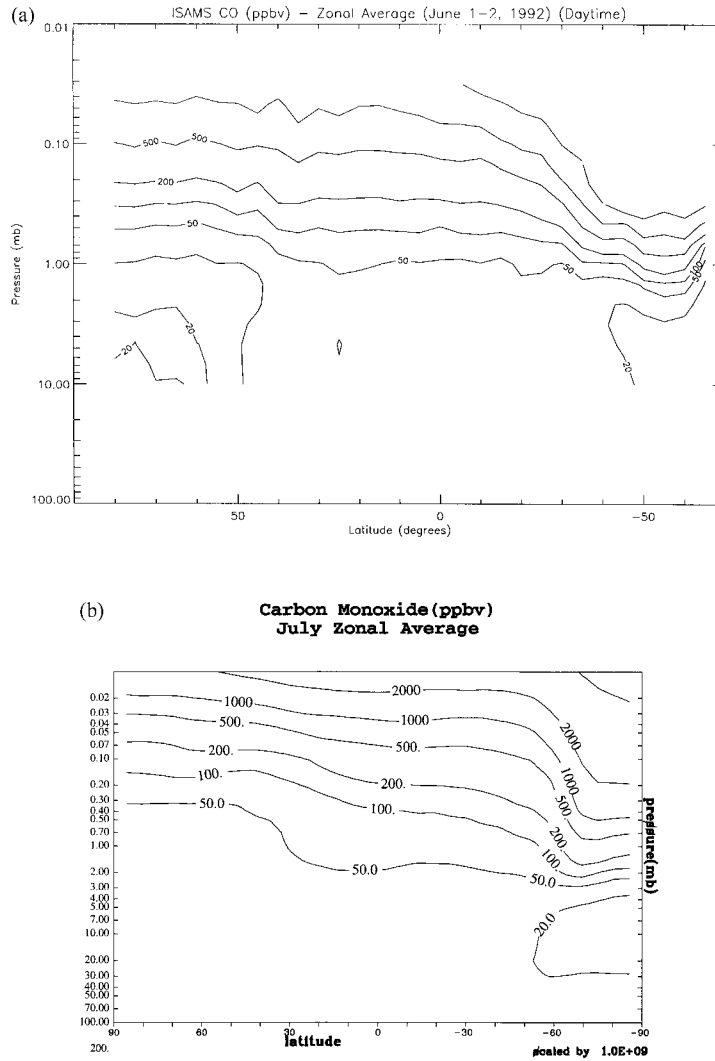July Zonal Average

(b)

Fig. 14   (a) ISAMS June 1992 zonal average of CO in ppbv and (b) CMAM July zonal average of CO in ppbv.

1997). Furthermore, not only are models able to predict closely species densities but are also able to reproduce some interesting dynamical characteristics such as the seasonal variation in stratospheric humidity levels known as the "tape recorder" effect (Section 2). Figure 15 shows equatorial total hydrogen levels and how they vary with pressure and time over a three year CMAM simulation.
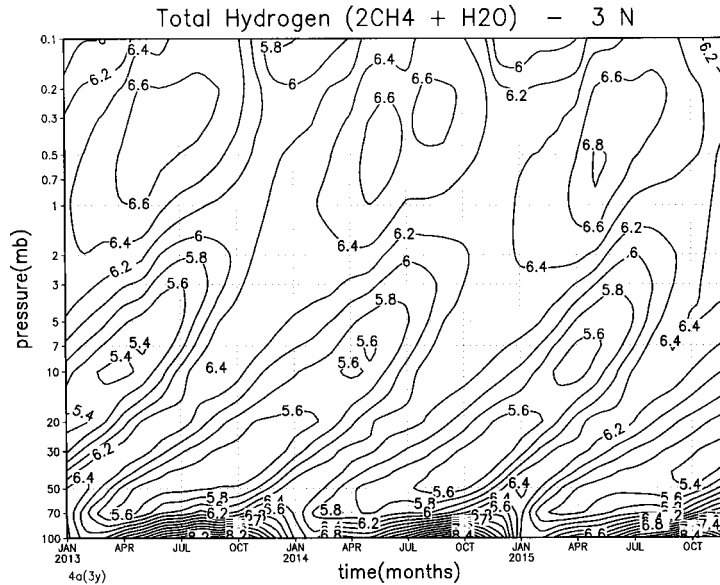
Fig. 15 Equatorial total hydrogen as a function of pressure and time (over three years). Note the annual "tape recorder" effect emanating from the tropopause and reaching up to altitudes of about 1 mb (~50 km). This variation in humidity levels is a result of changing tropopause temperature. The tropopause is the coldest point in the lower atmosphere. These low temperatures in effect "freeze out" much of the water being transported from the troposphere to the stratosphere.

b *Ozone*

1 PRELIMINARY COMMENTS

Figure 16 shows the zonally averaged concentration of ozone in ppmv as measured by the Microwave Limb Sounder (MLS) aboard UARS. Note that the mixing ratio profile peaks at about 10 mb (~31 km) while the higher mixing ratios are skewed towards the summer pole. Plotted as density, the (density) peak over the tropics occurs at about 25 km: 20 km at higher latitudes.

The behaviour of column ozone with latitude and season is shown in Fig. 17. Column ozone is defined as the vertically integrated amount of ozone in a column of unit area. Often column ozone is presented in Dobson units (DU), which would be the height of the entire column of ozone at 1 atmosphere pressure and 273 K (STP) in units of one one-hundredth of a millimetre. (One Dobson unit equals 2.69×10^{16} molecules cm^{-2} under these conditions.) Panel (a) shows the ten-year average column as predicted by the CMAM using a second generation version of the model (S. Beagley and J. de Grandpré, personal communication) while panel (b) is the measured column ozone as given by CIRA (Cospar International Reference Atmosphere). One can see the year-round low amounts ~250 DU over the tropics; and at ~60°, the spring peak in both hemispheres with larger amounts in the Northern
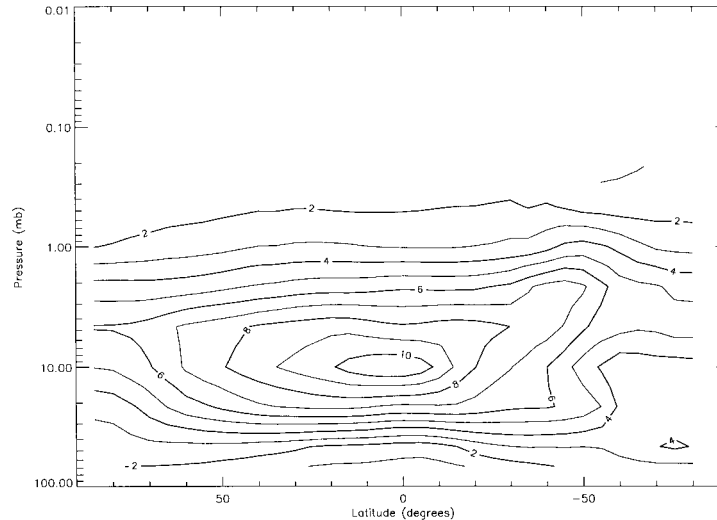
Fig. 16   July zonal average of ozone as measured by the Microwave Limb Sounder aboard the UARS satellite. Note the winter hemisphere upwelling near 50°S. The maximum ozone contour is at approximately 10 mb (31 km) with the contours skewed towards the summer pole.

Hemisphere. The lowest high latitude columns occur in the fall/autumn. In general, the model reproduces well the magnitude of ozone levels in both the winter and summer hemispheres except in the polar regions.

Figures 18a–f show the important terms in the July ozone budget using the CMAM model (de Grandpré et al., 1997). As noted earlier, we also see the large production at about 2 mb when there is 24 hours of sunlight at the North Pole. It can be seen that the different catalytic cycles are important at different heights. The NO_x family is the most important ozone sink in the lower to mid-stratosphere while the HO_x sink becomes more important at higher altitudes, as does the Chapman mechanism. The halogen family maxima occur in the same region where there is a maximum of ozone production. (Note different scaling factor for panel (f).) Most of the excess ozone is transported to high latitudes and through the tropopause where it represents an important term in the tropospheric ozone budget.

2 MODELLED AND OBSERVED TRENDS

Seasonally and annually averaged ozone decadal trends are shown in Fig. 19 as a function of latitude between about 60°S to 60°N. These ozone measurements are from ground-based sondes. Ozone has not declined noticeably over the tropics whereas statistically significant decreases have occurred at mid- and higher latitudes. Decreases over Canada are as high as 7% per decade in the springtime (when fortunately, ozone columns are highest over Canada).

The agreement between observed and modelled trends will depend on a number

(a)

Ozone Column(DU) – 10 years

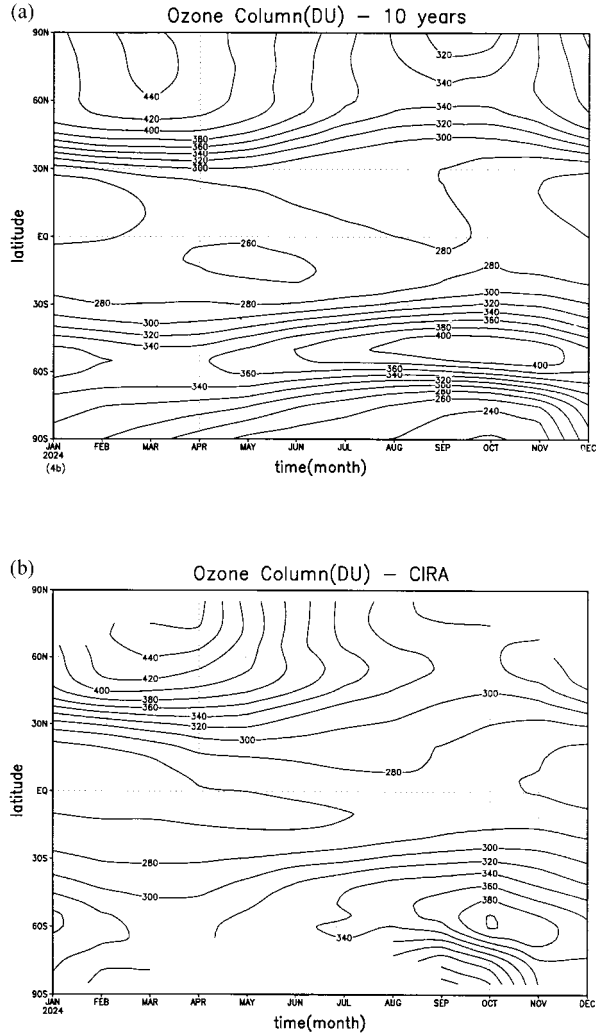(4b)

(b)

Ozone Column(DU) – CIRA

Fig. 17   Annual variation in ozone column amount in Dobson units for (a) CMAM (10-year average) (b) Observed (CIRA)

of factors. Solomon et al. (1998) has recently shown that good agreement with observed mid-latitude trends can be obtained with the current understanding of heterogeneous chemistry, when used together with anthropogenic halogen trends and wave-driven fluctuations in stratospheric temperatures. Also, the ability to predict correctly ozone trends is strongly dependent on volcanic activity, which can affect the atmosphere in a number of ways.

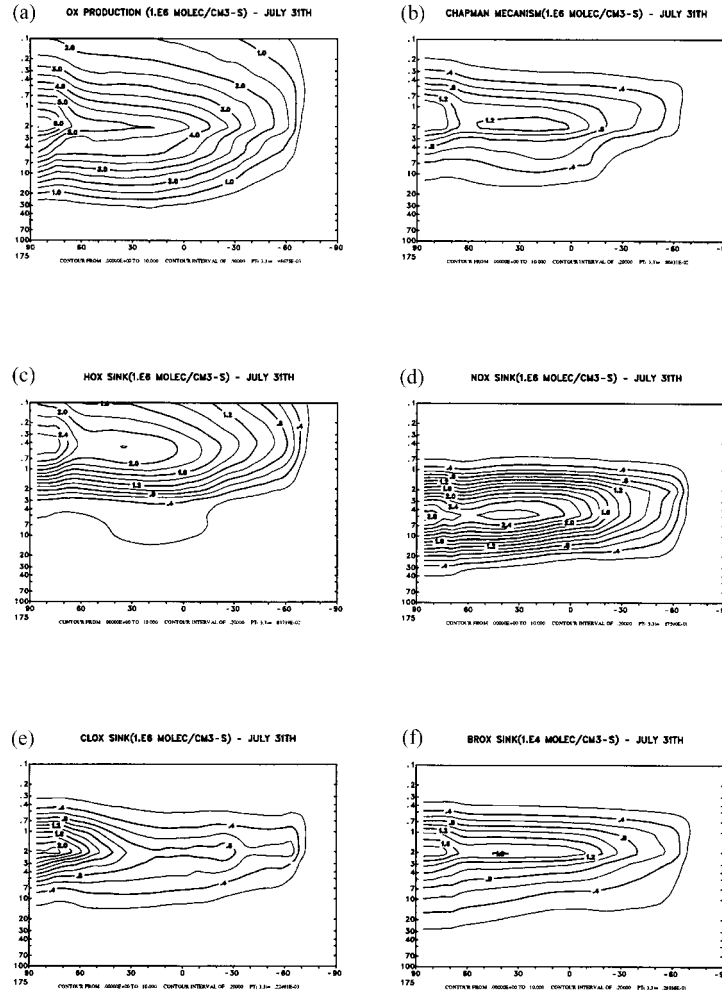A tremendous natural phenomenon occurred in the stratosphere when the erup-

Fig. 18   The ozone budget (10^6 molecules cm^{-3} s^{-1}) for July from the CMAM: (a) O_3 production from O_2 photolysis. Loss processes for ozone: (b) Chapman loss $O + O_3$ (c) HO_x reactions (d) NO_x reactions, (e) ClO_x reactions, (f) (10^4 molecules cm^{-3} s^{-1}) BrO_x reactions.

tion of Mt. Pinatubo began on 15 June 1991, resulting in the injection of about 18 MT of SO_2 (Cole-Dai et al., 1997) into the stratosphere and the subsequent generation of sulfate aerosols (c.f. Fig. 8). Simulations of this phenomenon indicate that sulfate aerosols led to the heating of the stratosphere and cooling of the troposphere (Hansen et al., 1992). Rosenfield et al. (1997) calculated a low-latitude stratospheric warming peak of 2.5 K in mid-1992 and high-latitude cooling of 1–2 K associated with high-latitude ozone reduction.
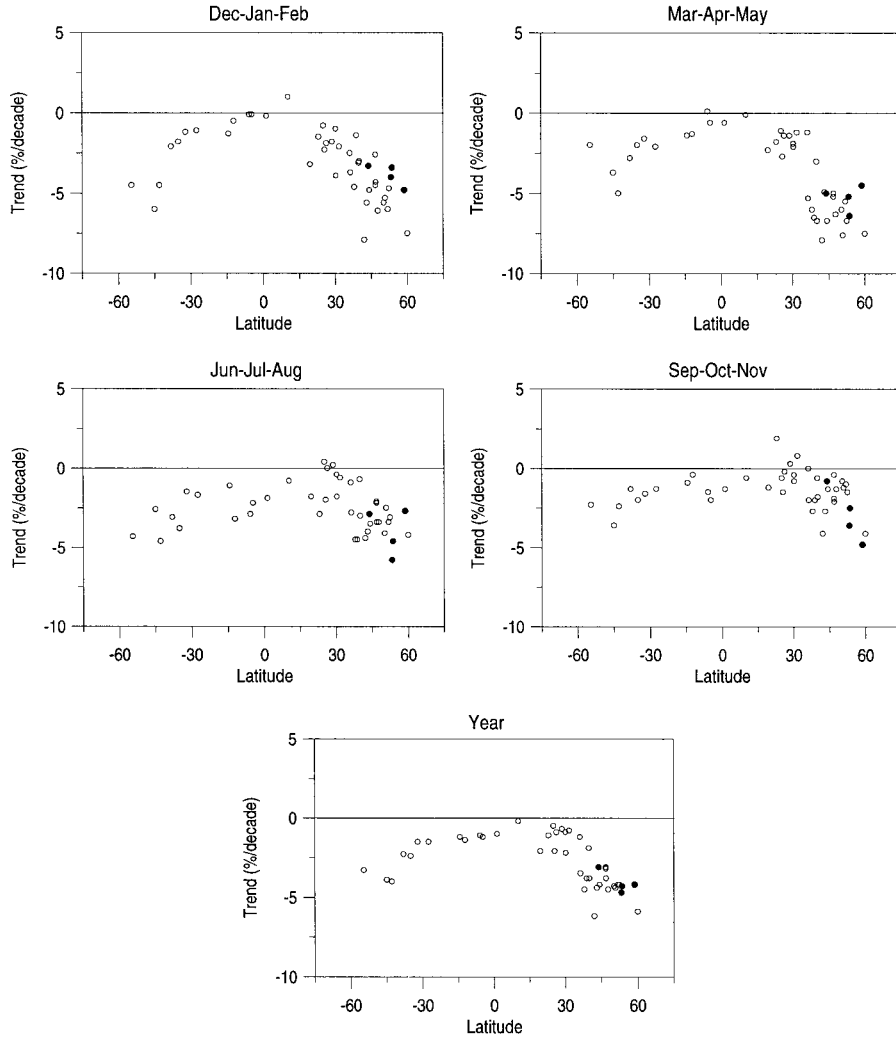
Fig. 19 Decadal trends in the annual and seasonal total ozone averages by latitude, from ground-based data (D. Tarasick and V. Fioletov, personal communication). The Canadian stations with long term records are indicated with solid circles. The trends are corrected for annual, quasi-biennial oscillations (QBO) and solar cycle variations.

Ozone was also affected by virtue of the perturbation of the nitrogen reservoirs by the conversion of N_2O_5 into HNO_3 within the sulfate aerosols, which in turn affected the Cl_x and to some extent the Br_x reservoirs. Furthermore, because of the generation of HOBr and production of OH, the lower stratospheric budget was greatly perturbed (Danilin and McConnell, 1995; Lary et al., 1996). Additionally, the heating

altered the transport patterns and the dynamical lifetimes of the ozone and, as a result, loss processes could act for longer periods. This dynamical perturbation affects the interannual variability, and makes determination of statistically significant trends more difficult (Jackman et al., 1996; Chandra et al., 1996).

More recently, much more attention is being paid to springtime ozone loss over the Arctic (e.g., Donovan et al., 1997; Lefèvre et al., 1998). This topic is especially important because the Arctic vortex is usually not centred over the pole as it is in the Antarctic but can reach to the higher mid-latitudes. The climatological location of the Arctic vortex tends to be dislocated from the pole and towards Europe because of ridging associated with the Aleutian anticyclone. The ridging itself is partly related to the position and topography of the continents as well as land-sea temperature contrasts (J. Fyfe, personal communication, 1998). However, the relative amount of ozone destruction is generally less than that found over the South Pole, due to a weaker and shorter-lived vortex and in general warmer temperatures (by about 10 K) resulting from stratospheric warmings. The vortex is often perturbed by large amplitude planetary-scale disturbances (Pierce et al., 1997).

Occasionally, however, the Arctic vortex is as strong and lasts as long as the Antarctic vortex as was the case in 1995-96, or lasts well into the spring, coupled with low temperatures as was the case in 1996-1997 (e.g., Newman et al., 1997). If the Arctic vortex displays characteristics similar to the Antarctic vortex, processing of reservoir chlorine species and concomitant ozone destruction of a similar magnitude can also take place. It has been shown recently that the depleted late-winter and early springtime ozone values in the Arctic are strongly correlated with unusually cold and protracted stratospheric winters, as well as more isolated vortices associated with weaker planetary wave driving (WMO, 1999).

The decrease in Arctic ozone is most severe in the spring as can be seen from the ground and from satellites. Measurements of the total ozone column obtained from satellite-based Total Ozone Mapping Spectrometer (TOMS) instruments shows this decrease (averaged over the entire polar region) in the month of March. In March 1997, the ozone column was 21% less than normal and in a small region near the pole the decrease was 40% (Newman et al., 1997). Although dynamics plays a major role in redistributing ozone in the Arctic stratosphere, it seems clear that chemical loss of ozone due to heterogeneous chemistry is playing a major role. In fact, several recent publications have indicated that much of the chemical loss in the winter and springtime Arctic is often masked by transport of ozone-rich air from above (Muller et al., 1997; Rex et al., 1997; Knudsen et al., 1998; Lefèvre et al., 1998). Specifically Muller et al. (1997) estimate that 120–160 DU of ozone were chemically destroyed between January and March 1996, overwhelming the putative dynamical increase leading to a net loss of about 50 DU. This chemical loss is greater than that which was occurring over Antarctica when the ozone hole was first observed in 1985 (Farman et al., 1985). However, the ozone-poor air is transported to lower latitudes and will modify the ozone budget in these regions. The ability to capture the details of this process

accurately in a detailed simulation does not yet exist but must certainly be developed for the next generation of models.

The modelling of ozone depletion over the poles requires processing of reservoir species on PSC surfaces when the temperature become cold enough. Generally, ozone depletion in the Antarctic is well represented by models but, in the Arctic, the situation seems less clear. Processing, as calculated from the ozone loss, appears to be too low by about 40% (Goutail et al., 1999). As we have noted, this may indicate a problem with the limited resolution of the CTMs used to date rather than a limitation of our knowledge of the chemistry (Edouard et al., 1996) although very recent studies have cast some doubt on this conclusion (Searle et al., 1998).

In addition, because the Arctic temperatures are higher than those in the Antarctic, knowledge of temperatures appears to be much more critical for calculating Arctic ozone depletion: a few degrees can make a substantial difference in the extent of processing. In particular, there is uncertainty regarding the lowest values at which PSCs will form in the Arctic. It should be noted that there is a significant cooling occurring in the polar lower stratosphere of ~3 K per decade, although the dynamical variability in this region is substantial. This makes future Arctic ozone levels particularly sensitive to small changes in local temperature (WMO, 1999). Furthermore, Pullen and Jones (1997) compared objectively analysed (OA) temperatures from the U.K. Meteorological Office (UKMO) with independent sonde measurements and found that the OA temperatures are often too high by 1 to 2 degrees at the lowest values. Similar offsets are found for the lowest (European Centre for Medium Range Weather Forecasting) ECMWF temperatures in the Arctic (Knudsen, 1996). Also, it is not clear if most models capture the different temperature scales within the Arctic: for example, as noted earlier, PSCs can be induced by flow over mountains which is a mesocale phenomenon not directly addressed in most models to date. These localized PSC formation and processing events offer a possible explanation for the discrepancies between observed and previously modelled ozone concentrations (Carslaw et al., 1998). This effect is quite different from the scale effects introduced by the filamentation processes associated with dynamics.

As noted above, current models do quite well in reproducing the general behaviour of total ozone columns in the atmosphere (McPeters et al., 1996; Jackman et al., 1996; Rasch et al., 1995; Solomon et al., 1998). Nevertheless, there still appears to be a disagreement between calculated and measured ozone levels near the stratopause, with the models overestimating ozone loss by about 30% (e.g., Minschwaner et al., 1993; Osterman et al., 1997). Careful comparison has also revealed discrepancies between modelled and observed ratios of active to reservoir species for Cl_y. However, a recent modelling study by Khosravi et al. (1998) indicates that decreasing the rate of

$$HO_2 + O \rightarrow OH + O_2 \tag{123}$$

and providing for a 6% minor branch for the reaction

$$ClO + OH \rightarrow HCl + O_2 \qquad\qquad (124)$$

(both of which are within experimental errors), along with constraining temperatures and CH_4 to those observed by the UKMO provides satisfactory agreement between observations and their 3D model.

3 FUTURE OZONE

The future trends in ozone levels will be affected directly by CFC (chlorofluorocarbon) emissions. The reduction of these environmentally harmful gases was the subject of an international meeting in Montréal in 1987, at which the Montréal Protocol was adopted. It was recognized that CFC-11 and CFC-12 are major sources of chlorine atoms in the lower stratosphere, and therefore major contributors to global ozone depletion. In recent years, there appears to be a levelling of both CFCs as shown in Fig. 20. The top panel shows the tropospheric concentration of CFC-11 reaching a maximum concentration of ~275 ppt in about 1992 and the levels may now be decreasing somewhat. The lower panel shows present-day CFC-12 levels to be about 550 ppt and although it is not clear that the concentration has reached a maximum, it is certain that the rate is decreasing and may soon level off. If the provisions of the Montréal Protocol are followed, peak present day stratospheric Cl concentrations of ~3.7 pptv will eventually return to their normal levels of less than 1 pptv by the end of the 21st century or soon after (Elkins et al., 1993; WMO, 1999; Engel et al., 1998).

In a recent article, however, Shindell et al. (1998) used a Global Climate/Middle Atmospheric Model (GCMAM) with simplified chemistry and constrained ozone transport to investigate the coupling between chemistry and climate. For the period 2010–2019, increased greenhouse gas emissions caused a decrease in temperature of 1–2 K due to radiative cooling poleward of 70°N. Also, there was an additional 8–10 K cooling due to an increased stability of the Arctic vortex compared to present day temperature climatology. This dramatic decline in stratospheric temperatures in their model caused an Arctic ozone hole in the spring with a 2/3 loss of the total ozone column, in spite of anticipated decreases of CFC concentrations because of the implementation of the Montréal Protocol. The possibility of an Arctic ozone hole is a very disturbing development with strong political and social implications. In contrast to the Antarctic ozone hole, an Arctic ozone hole would effect heavily populated parts of the Northern Hemisphere.

c *Aircraft Emissions*

Anthropogenic emissions of species into the upper troposphere and lower stratosphere by fleets of subsonic and supersonic aircraft have received increasing attention over the past few years (e.g., WMO, 1994; Lary et al., 1997). It is known that the burning of hydrocarbon fuels by these aircraft emits water vapour, methane, NO_x, CO, sulfur oxides as well as particulate matter. The environmental conse-
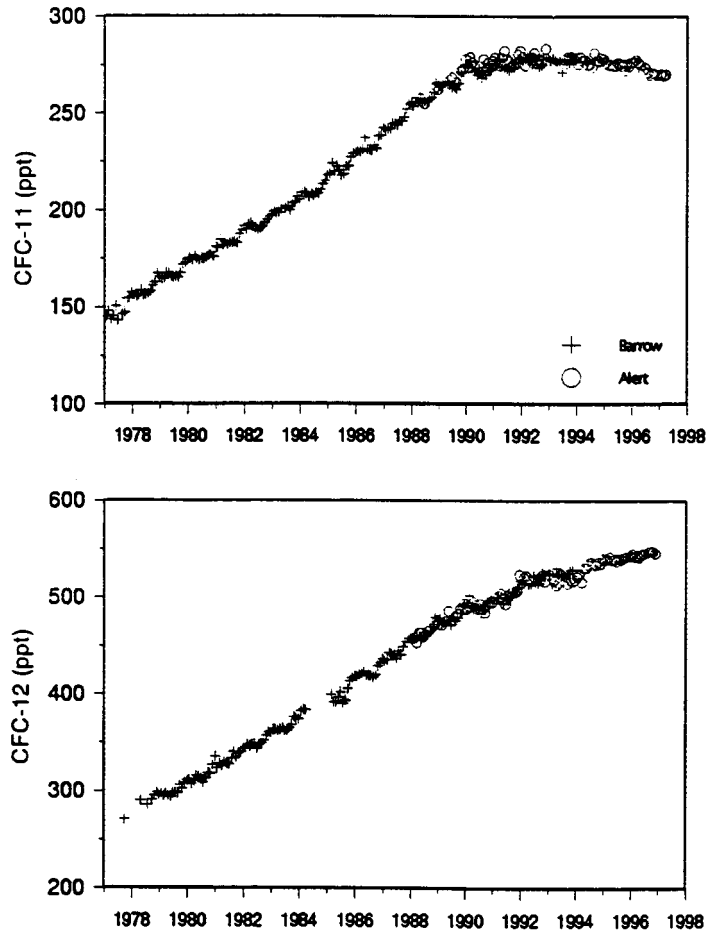
Fig. 20 Measurements of tropospheric CFC concentrations from samples taken at Barrow and Alert in the Canadian Arctic (J.W. Elkins, personal communication).

quence of the emissions is a matter of concern as air travel is expected to substantially increase in the years to come (Brasseur et al., 1998).

The present and projected fleet of High Speed Civil Transport (HSCT) aircraft flying at supersonic speed in the lower stratosphere was also studied to determined how it would perturb ozone concentrations. It was found that the amount of effluent SO_2 which is converted to aerosol particles and subsequently to total surface area density has a large influence on the calculated ozone response. For example, when no sulfur is injected into the aircraft plume and no aerosol formation takes place, the ozone level drop is $\leq 0.4\%$, while a 50% SO_2 gas to particle conversion causes a

change in ozone level between 0.5% to –1.3%. Clearly, the microphysics of nucleation in the highly perturbed and non-equilibrium conditions of an aircraft engine plume needs to be further examined.

A recent model comparison between several two- and three-dimensional chemistry transport models was undertaken to address the above concerns (Isaken and Jackman, 1998). Using a standard atmosphere as model initial conditions and predicting future aircraft use and engine effluent, these models attempted to predict future NO_x and ozone response to a fleet of subsonic aircraft in the years 1992, 2015 and 2050. The main perturbation to global ozone levels is expected to be in the area of 10 to 12 km altitude and in a latitude band between 30–60°N, due to greater aircraft traffic. This indeed appears to be the case with zonally averaged ozone levels predicted to increase by approximately 5 ppbv at this altitude and latitude in the year 1992. By 2015, the increase in ozone levels attributable to aircraft emissions is approximately 8 ppbv, and about 13 ppbv in the year 2050. NO_x level perturbations range from 50–150 pptv at 12 km at boreal mid-latitudes.

Carbon aerosols are a by-product of combustion processes. Much recent activity in atmospheric modelling has addressed the possible influence of commercial aircraft and their emissions on the chemical balance of the lower stratosphere and upper troposphere, especially at mid-latitudes. Due to the aircraft source of carbon soot particles, there is expected to be a north-south asymmetry in the chemical effects (Lary et al., 1997). Carbon soot is thought to be morphologically quite different from sulfate aerosols. While the latter are essentially spherical, the former is thought to be composed of chain aggregates of small $\sim$20 nm diameter spheres. The total surface area for these string-like structures can be upwards of 20 times greater than if the particles were spherical (Bekki, 1997).

The reactions which are thought to occur on carbon soot are:

$$O_3 \xrightarrow{C} products \qquad\qquad (125)$$

$$HNO_3 \xrightarrow{C} NO_x + products. \qquad\qquad (126)$$
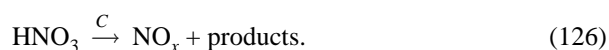
The ozone depletion reaction has a γ of 0.0033 as suggested by DeMore et al. (1997) but the uncertainty in this number is quite large, with the reaction probability varying quite strongly with the surface history of the carbon soot which may be subject to saturation of available reaction sites (Chughtai et al., 1996). The products have been determined to be CO, CO_2 and O_2. The HNO_3 reduction has a suggested an uptake probability of 0.04 with two-thirds of the measured HNO_3 uptake producing NO and NO_2 (DeMore et al., 1997). These reactions are temperature independent and do not require the presence of light in order for either reaction to occur.

In order to investigate the effects of these reactions on NO_x and ozone balance, some recent studies have incorporated them into 2D and 3D models. Bekki (1997) found that at northern mid-latitudes, there is overall local ozone production below about 10 km (300 mb) of about 0.2% per year, while above this level, ozone is

depleted by about 0.4% per year. The HNO_3 reduction reaction served to increase the NO_2/HNO_3 ratio by as much as 200% at high northern latitudes in the winter at about 12 to 15 km. He concluded that the equations are able to reproduce a large part of the trend in mid-latitude ozone depletion but warned that the results are sensitive to the ozone uptake coefficient. He also concluded that this mechanism of regenerating NO_x from a nitrogen reservoir species, HNO_3, (called *renoxification*) cannot account for most of the possible discrepancies between the observed and modelled NO_y partitioning. It has also been suggested that the effect of carbon aerosols is unlikely to be catalytic in nature (Isaken and Jackman, 1998).

7 Summary

The myriad of chemical and photochemical reactions taking place in the stratosphere is an extremely complex system. These reactions can take place either in the gas phase or can occur on/in heterogeneous surfaces which can be formed from source gases such as SO_2, H_2O or HNO_3. The stratosphere is very important to the biosphere because of the protective ozone layer, which along with O_2, H_2O and CO_2 are able to absorb much of the harmful ultraviolet radiation from the sun. Changes in ozone levels also have a dramatic effect on other phenomena in the atmosphere. Changes in ozone concentrations can alter radiative heating which can lead to temperature gradients which create increased wind speeds which affect the transport of chemical species, including ozone itself. Changes in local temperature can affect the rates of many temperature dependent reactions, such as the important $O + O_3 \rightarrow 2O_2$ reaction. Also, a decrease in temperature can increase the amount of adsorbed/dissolved HCl on aerosol or PSC particles, which can lead to an increase in ozone destruction.

Accurate modelling of ozone and other trace species in the stratosphere is of prime importance for all CTMs and AGCMs. Ozone levels are well predicted over the Antarctic: the phenomenon of the ozone hole in the spring is well simulated by current models which include processing on PSCs. The polar vortex which forms over the Arctic is not as strong as that found over the South Pole and the temperatures are not as cold in general. Simulations of North Pole ozone depletion are not as accurate as those found over the South Pole due to the more complex interplay between dynamics and chemistry in this region of the globe. Mid-latitude stratospheric ozone concentrations are usually underestimated by current models but there is no evidence that the chemistry in this region is lacking but rather may be a shortcoming in our ability to simulate equatorial dynamics (Folkins et al., 1996). The future trends in ozone levels are also a very important research topic with tremendous social, political and economic implications. A very preliminary study suggests that ozone levels over the Arctic will continue to decrease, with the largest decrease occurring sometime around 2015, even with the adherence to guidelines set forth in the Montréal Protocol. This is clearly an area which requires further study.

The chemistry and dynamics of the stratosphere and indeed all regions of the

atmosphere continue to be a very important field of study. Considerable research continues to be done on all topics addressed in this survey. The determination of the rates of various important (or previously neglected) chemical reactions, the effects of a variety of anthropogenic and biogenic emissions, and new (or previously neglected) dynamical and radiative influences are all areas which require refinement in order to obtain better agreement with trace species measurements and as such "verify" the model.

Acknowledgements

References

ANDERSON, J.G.; D.W. TOOHEY and W.H. BRUNE. 1991. Free radicals within the Antarctic vortex: the role of CFCs in Antarctic ozone loss. *Science*, **251**: 39–46.

BEKKI, S. 1997. On the possible role of aircraft-generated soot in the middle latitude ozone depletion, *J. Geophys. Res.* **102**: 10751–10758.

BRASSEUR, G. and S. SOLOMON. 1986. *Aeronomy of the Middle Atmosphere*, D. Reidel, Dortrecht, Holland.

——— and C. GRANIER. 1992. Mount Pinatubo aerosols, chlorofluorocarbons, and ozone depletion. *Science*, **257**: 1239–1242.

———; X. TIE, P. RUSCH and F. LEFÈVRE. 1997. A three-dimensional simulation of the Antarctic ozone hole: Impact of anthropogenic chlorine on the lower stratosphere and upper troposphere. *J. Geophys. Res.* **102**: 8909–8930.

———; R.A. COX, D. HAUGLUSTAINE, I. ISAKEN, J. LELIEVELD, D.H. LISTER, R. SAUSEN, U. SCHUMANN, A. WAHNER and P. WIESEN. 1998. European Scientific Assessment of the Atmospheric Effects of Aircraft Emissions. *Atmos. Env.* **32**: 2327–2422.

CARSLAW, K.S.; B.P. LUO, S.L. CLEGG, T. PETER, P. BRIMBLECOME and P.J. CRUTZEN. 1994. Stratospheric aerosol growth and HNO_3 gas phase depletion from coupled HNO_3 and water uptake by liquid particles. *Geophys. Res. Lett.* **21**: 2479–2482.

———; ———, and T. PETER. 1995. An analytic expression for the composition of aqueous HNO_3-H_2SO_4 stratospheric aerosols including gas phase removal of HNO_3. *Geophys. Res. Lett.* **22**: 1877–1880.

———; M. WIRTH, A. TSIAS, B.P. LUO, A. DORN-BRACK, M. LEUTBECHER, H. VOLKERT, W. RENGER, J.T. BACMEISTER, E. REIMER and T. PETER. 1998. Increased stratospheric ozone depletion due to mountain-induced atmospheric waves. *Nature*, **391**: 675–678.

CHANDRA, S.; C. VAROTSOS and L.E. FLYNN. 1996. The mid-latitude total ozone trends in the northern hemisphere. *Geophys. Res. Lett.* **23**: 555–558.

CHAPMAN, S. 1930. A theory of upper atmospheric ozone. *Q.J.R. Meteorol. Soc.* **3**: 103–125.

CHARTRAND, D.J. and J.C. MCCONNELL. 1998. Evidence for HBr production due to minor channel branching at mid-latitudes. *Geophys. Res. Lett.* **25**: 55–58.

CHIPPERFIELD, M.P., E.R. LUTMAN, J.A. KETTLEBOROUGH, J.A. PYLE and A.E.ROCHE. 1997. Model studies of chlorine deactivation and formation of ClONO$_2$ collar in the Arctic polar vortex. *J. Geophys. Res.* **102**: 1467–1478.

CHUGHTAI, A.R.; M.R. BROOKS and D.M. SMITH. 1996. Hydration of black carbon. *J. Geophys. Res.* **101**: 19505–19514.

CLARY, D.C. 1996. Molecules on ice. *Science*, **271**: 1509.

CLYNE, M.A.A. and R.T. WATSON. 1977. Kinetic studies of diatomic free radicals using mass spectrometry. *J. Chem. Phys.* **1/73**: 1169–1187.

COLE-DAI, J.; E. MOSLEY-THOMPSON and L.G. THOMPSON. 1997. Quantifying the Pinatubo volcanic effect in south polar snow. *Geophys. Res. Lett.* **24**: 2679–2682.

DANILIN, M.Y. and J.C. MCCONNELL. 1995. Stratospheric effects of bromine activation on/in sulfate aerosol. *J. Geophys. Res.* **100**: 11237–11243.

DE GRANDPRÉ. J.; J.W. SANDILANDS, J.C. MCCONNELL, S.R. BEAGLEY, P. CROTEAU and M.Y. DANILIN. 1997. Canadian Middle Atmosphere Climate Model: Preliminary Chemistry Results. ATMOSPHERE-OCEAN, **35**: 385–431.

DEMORE, W.B.; S.P. SANDER, D.M. GOLDEN, R.F. HAMPSON, M.J. KURYLO, C.J. HOWARD, A.R. RAVISHANKARA, C.E. KOLB and M.J. MOLINA. 1997. Chemical Kinetics and Photochemical Data for use in Stratospheric Modeling, JPL Publication 97-4, Pasadena, CA. 266 pp.

DONALDSON, D.J.; A.R. RAVISHANKARA and D.R. HANSON. 1997. Detailed study of HOCl + HCl → Cl$_2$ + H$_2$O in sulfuric acid. *J. Phys. Chem.* **101**: 4717–4725.

DONOVAN, D.P.; H. FAST, Y. MAKINO, J.C. BIRD, A.I. CARSWELL, J. DAVIES, T.J. DUCK, J.W. KAMINSKI, C.T. MCELROY, R.L.M. MITTERMEIER, S.R. PAL, V. SAVASTIOUK, D. VELKOV and J.A. WITEWAY. 1997. Ozone, column ClO, and PSC measurements made at the NDSC Eureka observatory (80°N, 86°W) during the spring of 1997. *Geophys. Res. Lett.* **24**: 2709–2712.

DYE, J.E.; D. BAUMGARDNER, B.W. GANDRUD, S.R. KAWA, K.K. KELLY, M. LOWENSTEIN, G.V. FERRY, K.R. CHAN and B.L. GARY. 1992. Particle size distributions in Arctic polar stratospheric clouds, growth and freezing of sulfuric acid droplets, and implications for cloud formation. *J. Geophys. Res.* **97**: 8015–8034.

———; B.J. JOHNSON and W.R. ROZIER. 1993. Balloonborne measurements of Pinatubo aerosols during 1991 and 1992 at 41°N: Vertical profiles, size distribution, and velocity. *Geophys. Res. Lett.* **20**: 1435–1438.

EDOUARD, S.B.; B. LEGRAS, F. LEFEVRE and R. EYMARD. 1996. The effect of small scale inhomogeneities on ozone depletion in the Arctic. *Nature*, **384**: 444–447.

ELKINS, J.W; T.M. THOMPSON, T.H. SWANSON, J.H. BUTLER, D.B. HALL, S.O. CUMMINGS, D.A. FISHER and A.G. RAFFO. 1993. Decrease in the growth rates of atmospheric chloroflurocarbons-11 and -12. *Nature*, **364**: 780–783.

ENGEL, A.; U. SCHMIDT and D. MCKENNA. 1998. Stratospheric trends of CFC-12 over the past two decades: Recent observational evidence of declining growth rates. *Geophys. Res. Lett.* **25**: 3319–3322.

FARMAN, J.C.; B.G. GARDINER and J.D. SHANKLIN. 1985. Large losses of the total ozone in Antarctica reveal seasonal ClO$_x$/NO$_x$ interaction. *Nature*, **315**: 207–210.

FOLKINS, I.; G. BRASSEUR and C. GRANIER. 1996. Comparison of models of middle atmosphere composition with observations. *Adv. Space. Res.* **18**: 241–254.

FUCHS, N.A. and A.G. SUTUGIN. 1971. High dispersed aerosols. In: *Topics in Current Aerosol Research*, Vol. 6, G.M. Hidy and J.R. Brock (Eds), pp. 1–60, Permagon, New York.

GOUTAIL, F.; J.P. POMMEREAU, F. LEFEVRE, E. KYRO, M. RUMMUKAINEN, P. ERIKSON, S.B. ANDERSEN, B-A. KAASTAD-HOISKAR, G. BROATHEN, V. DOROKHOV and V.U. KHATTALOV. 1999. Depletion of column ozone in the Arctic during the winters of 1993–94 and 1994–95. *J. Atmos. Chem.* **32**: 1–34.

HANSEN, J.E. and L.D. TRAVIS. 1974. Light scattering in planetary atmospheres. *Space Sci. Rev.* **16**: 527–610.

———; A. LACIS, R. RUEDY and M. SATO. 1992. Potential climate impact of Mount Pinatubo eruption. *Geophys. Res. Lett.* **19**: 215–218.

HAYNES, D.R.; N.J. TRO and S.M. GEORGE. 1992. Condensation and evaporation of water ice surfaces. *J. Phys. Chem.* **96**: 8502–8509.

HOFMANN, D.J. 1990. Increase in the stratospheric background sulfuric acid aerosol mass in the past 10 years. *Science*, **248**: 996–1000.

HOLTON, J.R.; P.H. HAYNES, M.E. MCINTYRE, A.R. DOUGLAS, R.B. ROOD and L. PFISTER. 1995. Stratosphere-Troposphere exchange. *Rev. Geophys.* **33**: 404–439.

ISAKEN, I. and C. JACKMAN. 1999. Modeling the chemical composition of the future atmosphere. In: *Aviation and the Global Atmosphere*. J.E. Penner, D.H. Lister, D.J. Griggs, D.J. Dokkens and M. McFarland (Eds). IPCC Special Report, Chp 4. Cambridge University Press. pp. 121–163.

JACKMAN, C.H.; E.L. FLEMING, S. CHANDRA, D.B. CONSIDINE and J.E. ROSENFIELD. 1996. Past, present and future modeled ozone trends with comparisons to observed trends. *J. Geophys. Res.* **101**: 28753–28767.

JUCKS, K.W.; D.G. JOHNSON, K.V. CHANCE, W.A. TRAUB, R.J. SALAWITCH and R.A. STACHNIK. 1996. Ozone production and loss rate measurements in the middle stratosphere. *J. Geophys. Res.* **101**: 28785–28792.

KAMINSKI, J.W. and J.C. MCCONNELL. 1991. A note on the enhancement of J values in optically thick scattering atmospheres. *Can. J. Phys.* **69**: 1166–1174.

———; J.C. MCCONNELL, G. BRUNET, P. GAUTHIER and S. PELLERIN. 1999. Assimilation of Odin ozone data in the CMC weather forecast model with chemistry: Preliminary results. *In*: Proc. SODA Workshop on Chemical Data Assimilation. KNMI, de Bilt, 9–10 December 1998. KNMI pub. series 188. pp. 37–42.

KASTEN, F. 1968. Falling speed of aerosol particles. *J. Appl. Meteorol.* **7**: 944–947.

KHOSRAVI, R.; G.P. BRASSEUR, A.K. SMITH, D.W. RUSCH, J.W. WATERS and J.M. RUSSELL III. 1998. Significant reduction in the stratospheric ozone deficit using a three-dimensional model constrained with UARS data. *J. Geophys. Res.* **103**: 16203–16220.

KOOP, T. and K.S. CARSLAW. 1996. Melting of $H_2SO_4 \cdot 4H_2O$ particles upon cooling: Implications for polar stratospheric clouds. *Geophys. Res. Lett.* **25**: 3747–3750.

———; K.S. CARSLAW and T. PETER. 1997. Thermodynamic stability and phase transitions of PSC particles. *Geophys. Res. Lett.* **24**: 2199–2202.

KNUDSEN, B.M. 1996. Accuracy of Arctic stratospheric temperature analyses and the implications for the prediction of polar stratospheric clouds. *Geophys. Res. Lett.* **25**: 3747–3750.

———; M. LARSEN, I.S. MIKKELSEN, J.-J. MORCRITTE, G.O. BROATHE, E. KYRO, H. FAST, H. GERNANDT, H. KANZAW, H. NAKANE, V. DOROKHOV, Y. YUSHKOV, G. HANSEN, M. GIL and R.J. SHEARMAN. 1998. Ozone depletion in and below the Arctic vortex for 1997. *geophys. Res. Lett.* **25**: 627–630.

KROES, G.-J. and D. CLARY. 1992. Sticking of HCl and ClOH to Ice: A computational study. *J. Phys. Chem.* **96**: 7079–7088.

LARY, D.J. 1996. Gas phase atmospheric bromine photochemistry. *J. Geophys. Res.* **101**: 1505–1516.

———. 1997. Catalytic destruction of stratospheric ozone. *J. Geophys. Res.* **102**: 21515–21526.

———; M.P. CHIPPERFIELD, R. TOUMI and T.M. TENTON. 1996. Heterogeneous atmospheric bromine chemistry. *J. Geophys. Res.* **101**: 1489–1504.

———; A.M. LEE, R. TOUMI, M.J. NEWCHURCH, M. PIRRE and J.B. RENARD. 1997. Carbon aerosols and atmospheric photochemistry. *J. Geophys. Res.* **102**: 3671–3682.

LEFÈVRE, F.; F. FIGAROL, K.S. CARSLAW and T. PETER. 1998. The 1997 Arctic ozone depletion quantified from three-dimensional simulations. *Geophys. Res. Lett.* **25**: 2425–2428.

LELIEVELD, J.; B. BREGMAN, F. ARNOLD, V. BERGER, P.J. CRUTZEN, H. FISCHER, A. WAIBEL, P. SEIGMUND and P.F.J. VAN VELHOVEN. 1997. Chemical perturbation of the lowermost stratosphere through exchange with the troposphere. *Geophys. Res. Lett.* **24**: 575–578.

LOPEZ-VALVERDE, M.A.; M. LOPEZ-PUERTAS, J.J. REMEDIOS, C.D. ROGERS, F.W. TAYLOR, E.C. ZIPF and P.W. ERDMAN. 1996. Validation of measurements of carbon monoxide from the improved stratospheric and mesospheric sounder. *J. Geophys. Res.* **101**: 9929–9955.

MCCONNELL, J.C. and D.J. CHARTRAND. 1997. Ozone Chemistry: Simulation and Depletion. In: *Ozone Science: A Canadian Perspective on the Changing Ozone Layer*. D.I. Wardle, J.B. Kerr, C.T. McElroy and D.R. Francis (Eds). Environment Canada Publication, University of Toronto Press.

MCCORMICK, M.P. 1987. SAGE II: An overview. *Adv. Space Res.* **7**: 219–226.

MCELROY, M.B. and D.M. HUNTEN. 1966. A method of estimating the Earth albedo of dayglow measurements. *J. Geophys. Res.* **71**: 3635–3638.

MCPETERS, R.D.; S.M. HOLLANDSWORTH, L.E. FLYNN, J.R. HERMAN and C.J. SEFTOR. 1996. Long-term ozone trends derived from the 16-year combined Nimbus7/Meteor 3 TOMS Version 7 record. *Geophys. Res. Lett.* **23**: 3699–3702.

MICHELSON, H.A.; R.J. SALAWITCH, M.R. GUNSON, C. AELLIG, N. KAMPFER, M.M. ABBAS and M.C. ABRAMS. 1996. Stratospheric chlorine partitioning: constraints from Shuttle-borne measurement of [HCl], [ClNO$_3$], and [ClO]. *Geophys. Res. Lett.* **23**: 2361–2364.

MINSCHWANER, K.; R.J. SALAWITCH and M.B. MCELROY. 1993. Absorption of solar radiation by O$_2$: Implications for O$_3$ and lifetimes of N$_2$O, CFCl$_3$, and CF$_2$Cl$_2$, *J. Geophys. Res.* **98**: 10543–10561.

MLYNCZAK, M.G. and S. SOLOMON, 1993. A detailed evaluation of the heating efficiency in the middle atmosphere. *J. Geophys. Res.* **98**: 10517–10541.

MOLINA, L.T. and M.J. MOLINA. 1987. Production of Cl$_2$O$_2$ from the self-reaction of the ClO radical. *J. Phys. Chem.* **91**: 433–436.

MOTE, P.W.; K.H. ROSENKOF, M.E. MCINTYRE, E.S. CARR, J.C. GILLE, J.R. HOLTON, J.S. KINNERSLEY, H.C. PUMPHREY, J.M. RUSSELL III and J.W. WATERS. 1996. An atmospheric tape recorder: The imprint of tropical Tropopause temperatures on stratospheric water vapor. *J. Geophys. Res.* **101**: 3989–4006.

NEWMAN, P.A.; J.F. GLEASON, R.D. MCPETERS and R.S. STOLARSKI. 1997. Anomalously low ozone over the Arctic. *Geophys. Res. Lett.* **24**: 2689–2692.

OSTERMAN, G.B.; R.J. SALAWITCH, B. SEN, G.C. TOON, R.A. STACHNIK, H.M. PICKETT, J.J. MARGITAN, J-F BLAVIER and D.B. PETERSON. 1997. Balloon-borne measurements of stratospheric radicals and their precursors: Implications for the production and loss of ozone. *Geophys. Res. Lett.* **24**: 1107–1110.

PETER, T. 1997. Microphysics and heterogeneous chemistry of polar stratospheric clouds. *Ann. Rev. Phys. Chem.* **48**: 785–822.

PIERCE R.B.; T.D. FAIRLIE, E.E. REMSBERG, J.M. RUSSELL III and W.L. GROSS. 1997. HALOE observations of the Arctic vortex during the 1997 spring: Horizontal structure in the lower stratosphere. *Geophys. Res. Lett.* **24**: 2701–2704.

PLUMB, R.A. 1996. A "tropical pipe" model of stratospheric transport. *J. Geophys. Res.* **101**: 3957–3972.

PRATHER, M.J. 1986. Numerical advection by conservation of second-order moments *J. Geophys. Res.* **91**: 6671–6681.

PULLEN, S. and R.L. JONES. 1997. Accuracy of temperature from UKMO analyses of 1994/95 in the Arctic winter stratosphere *Geophys. Res. Lett.* **24**: 845–848.

RASCH, P.J. and D.L. WILLIAMSON. 1990. Computational aspects of moisture transport in global models of the atmosphere. *Q.J.R. Meteorol. Soc.* **116**: 1071–1090.

———; B.A. BOVILLE and G.P. BRASSEUR. 1995. A three–dimensional General Circulation Model with coupled chemistry for the middle atmosphere. *J. Geophys. Res.* **100**: 9041–9071.

REX, M.; R.P. HARRIS, P. VONDER GATHEN, R. LEHMANN, G.O. BRAATHEN, E. REIMER, A. BECK, M.P. CHIPPERFIELD, R. ALFIER, M. ALLAART, F. O'CONNOR, H. DIER, V. DOROKHOV, H. FAST, M. GIL, E. KYRO, Z. LITYNSHA, I.S. MIKKELSEN, M.G. MOLYNEUX, H. NAKANE, J. NOTHOLT, M. RUMMUKAINEN, P. VIALTE and J. WENGER. 1997. Prolonged stratospheric ozone loss in the 1995–1996 Arctic winter. *Nature,* **389**: 835–838.

ROSENFIELD, J.E.; D.B. CONSIDINE, P.E. MEADE, J.T. BACMEITER, C.H. JACKMAN and M.R. SCHOEBERL. 1997. Stratospheric effects of Mount Pinatubo aerosols studied with a coupled two–dimensional model. *J. Geophys. Res.* **102**: 3649–3670.

SALAWITCH, R.J.; S. WOFSY, P. WENNBERG, R. COHEN, J. ANDERSON, D. FAHEY, R. GAO, E.R. KEIM, E.L. WOODBRIDGE, R.M. STIMPFLE, J.P. KOPLOW, D.W. KOHN, C.R. WEBSTER, R.D. MAY, L. PFISTER, E.W. GOTTLIEB, H.A. MICHELSEN, G.K. YUE, M.J. PRATHER, J.C. WILSON, C.A. BROCK, H.H. JONSSON, J.E. DYE, D. BAUMGARDNER, M.H. PROFFITT, M. LOEWENSTEIN, J.R. PODOLSKE, J.W. ELKINS, G.S. DUTTON, E.J. HINSTA, A.E. DESSTER, E.M. WEINSTOCK, K.K. KELLY, K.A. BOERING, B.C. DAUBE, K.R. CHAN and S.W. BOWEN. 1994. The distribution of hydrogen, nitrogen, and chlorine radicals: Implications for the heterogeneous production of HNO$_2$. *Geophys. Res. Lett.* **21**: 2551–2554.

SCHOEBERL, M.R.; A.E. ROCHE, J.M. RUSSELL III, D. ORTLAND, P.B. HAYS and J.W. WATERS. 1997. An estimation of the dynamical isolation of the tropical lower stratosphere using UARS wind and trace gas observations of the quasibiennial

oscillation *Geophys. Res. Lett.* **24**: 53–56.

SEARLE, K.R.; M.P. CHIPPERFIELD, S. BEKKI and J.A. PYLE. 1998. The impact of spatial averaging on calculated polar ozone loss, 1. Model experiments. *J. Geophys. Res.* **103:** 25397–25408.

SEINFELD, J.H. and S.N. PANDIS. 1998. *Atmospheric Chemistry and Physics,* Wiley–Interscience, New York, 519 pp.

SESSLER, J.; P.GOOD, A.R. MACKENZIE and J.A. PYLE. 1996. What role do type 1 polar stratospheric cloud and aerosol parametrizations play in modelled lower stratospheric chlorine activation and ozone loss? *J. Geophys. Res.* **101**: 28817–28835.

SHINDELL, D.T.; D. RIND, and P. LONERGAN. 1998. Increased polar stratospheric ozone losses and delayed eventual recovery owing to increased greenhouse-gas concentrations. *Nature*, **392**: 589–592.

SLUSSER, J.R.; D.J. FISH, E.K. STRONG, R.L. JONES, H.K. ROSCOE and A. SARKISSIAN. 1997. Five years of NO_2 vertical column measurements at Faraday (65°S): Evidence for the hydrolysis of $BrONO_2$ on Pinatubo aerosols. *J. Geophys. Res.* **102**: 12987–12993.

SOLOMON, S.; R.R. GARCIA, F.S. ROWLAND and D.J. WUEBBLES. 1986. On the depletion of Antarctic ozone. *Nature*, **321**: 755–758.

———; S. BORRMANN, R.R. GARCIA, R. PORTMANN, L. THOMASON, L.R. POOLE, D. WINKER and M.P. MCCORMICK. 1997. Heterogeneous chlorine chemistry in the tropopause region. *J. Geophys. Res.* **102**: 21411–21429.

———; R.W. PORTMANN, R.R. GARCIA, W. RANDEL, F. WU, R. NAGATANI, J. GLEASON, L. THOMASON, L.R. POOLE and M.P. MCCORMICK. 1998. Ozone depletion at mid-latitudes: Coupling of volcanic aerosols and temperature variability to anthropogenic chlorine. *Geophys. Res. Lett.* **25**: 1871–1874.

TABAZADEH, A.; R.P. TURCO and M.Z. JACOBSON. 1994. A model for studying the composition and chemical effects of stratospheric aerosols. *J. Geophys. Res.* **99**: 12897–12914.

——— and O.B. TOON. 1996. The presence of metastable HNO_3/H_2O solid phases in the stratosphere inferred from ER-2 data. *J. Geophys. Res.* **101**: 9071–9078.

———; ——— and E.J. JENSEN. 1997. Formation and implications of ice particle nucleation in the stratosphere. *Geophys. Res. Lett.* **24**: 2007–2010.

THOMASON, L.W.; G.S.KENT, C.R. TREPTE and L.R. POOLE. 1997a. A comparison of stratospheric aerosol background periods of 1979 and 1989–1991. *J. Geophys. Res.* **102**: 3611–3616.

———; L.R. POOLE and T. DESHLER. 1997b. A global climatology of stratospheric aerosol surface area deduced from Stratospheric Aerosol and Gas Experiment II measurements: 1984–1994. *J. Geophys. Res.* **102**: 8967–8976.

TIE, X.; G. BRASSEUR, B. BRIEGLEB and C. GRANIER. 1994. Two-dimensional simulation of Pinatubo aerosols and its effect on stratospheric ozone. *J. Geophys. Res.* **99**: 20545–20562.

TOLBERT, M.A. 1996. Polar clouds and sulfate aerosols. *Science*, **272**: 1597.

VOLK, C.M.; J.W. ELKINS, D.W. FAHEY, R.J. SALAWITCH, G.S. DUTTON, J.M. GILLIGAN, M.H. PROFFIT, M. LOWESTEIN, J.R. PODOLSKE, K. MINSCHWANER, J.J. MARGITAN and K.R. CHAN. 1996. Quantifying transport between the tropical and mid-latitude lower stratosphere. *Science*, **272**: 1763–1768.

WAYNE, R.P. 1985. *Chemistry of Atmospheres*, 2nd edition. Claredon Press, Oxford. 447 pp.

WEISENSTEIN, D.K.; G.K. YUE, M. KO, N. SZE, J.M. RODRIGUEZ and C.J. SCOTT. 1997. A two-dimensional model of sulfur species in aerosols. *J. Geophys. Res.* **102**: 13019–13035.

WMO. 1994. Scientific Assessment of Stratospheric Ozone: 1994. Chp. 11. World Meteorological Organization Global Ozone Research and Monitoring Project. Report No. 37. Geneva, World Meteorological Organization.

———. 1999. Scientific Assessment of Ozone Depletion: 1998, Chp. 7. Global Ozone Research and Monitoring Project. Report No. 44. Geneva.

YUE, G.K. 1981. The formation and growth of sulfate aerosols in the stratosphere. *Atmos. Env.* **15**: 549–556.

——— and P. HAMILL. 1979. The homogeneous nucleation rates of H_2SO_4 aerosol particles in air. *J. Aerosol Sci.* **10**: 10609–10614.

YUNG, Y.L.; J.P. PINTO, R.T. WATSON and S.P. SANDER. 1980. Atmospheric bromine and ozone perturbations in the lower stratosphere. *J. Atmos. Sci.* **37**: 339–353.

ZHAO, X.; R.P. TURCO, C.-Y.J. KAO and S. ELLIOT. 1997. Aerosol-induced chemical perturbations of stratospheric ozone. Three-dimensional simulations and analysis of mechanisms. *J. Geophys. Res.* **102**: 3617–3637.